Article

MD Simulations and FRET Reveal an Environment-Sensitive Conformational Plasticity of Importin-β

Kangkan Halder,[1] Nicole Dölker,[2] Qui Van,[3] Ingo Gregor,[3] Achim Dickmanns,[4] Imke Baade,[5] Ralph H. Kehlenbach,[5] Ralf Ficner,[4] Jörg Enderlein,[3] Helmut Grubmüller,[2,*] and Heinz Neumann[1,*]

[1]Free Floater (Junior) Research Group "Applied Synthetic Biology", Institute for Microbiology and Genetics, Georg-August University Göttingen, Göttingen, Germany; [2]Department of Theoretical and Computational Biophysics, Max-Planck Institute for Biophysical Chemistry, Göttingen, Germany; [3]Third Institute of Physics-Biophysics, [4]Institute for Microbiology and Genetics, Department of Molecular Structural Biology, and [5]Department of Molecular Biology, Faculty of Medicine, Georg-August University Göttingen, Göttingen, Germany

ABSTRACT The nuclear pore complex mediates nucleocytoplasmic transport of macromolecules in eukaryotic cells. Transport through the pore is restricted by a hydrophobic selectivity filter comprising disordered phenylalanine-glycine-rich repeats of nuclear pore proteins. Exchange through the pore requires specialized transport receptors, called exportins and importins, that interact with cargo proteins in a RanGTP-dependent manner. These receptors are highly flexible superhelical structures composed of HEAT-repeat motifs that adopt various degrees of extension in crystal structures. Here, we performed molecular-dynamics simulations using crystal structures of Importin-β in its free form or in complex with nuclear localization signal peptides as the starting conformation. Our simulations predicted that initially compact structures would adopt extended conformations in hydrophilic buffers, while contracted conformations would dominate in more hydrophobic solutions, mimicking the environment of the nuclear pore. We confirmed this experimentally by Förster resonance energy transfer experiments using dual-fluorophore-labeled Importin-β. These observations explain seemingly contradictory crystal structures and suggest a possible mechanism for cargo protection during passage of the nuclear pore. Such hydrophobic switching may be a general principle for environmental control of protein function.

INTRODUCTION

Fundamental processes, such as transcription and translation, depend on molecules crossing the nuclear envelope in both directions. The sites of transition are the nuclear pore complexes (NPCs) (1), which permit the passive passage of metabolites and small proteins (2,3). The central channel of the NPC is a hydrophobic meshwork formed by nucleoporins (4), which contain intrinsically disordered regions of phenylalanine-glycine (FG)-rich repeats (5). Macromolecules larger than ~40 kDa require specialized receptors as transport mediators to traverse the permeability barrier of the nuclear envelope efficiently (6–8), although exceptions are known for larger proteins with unusual surface hydrophobicity (9,10).

Most of the proteins that mediate nuclear transport belong to the homologous Importin-β/Karyopherin superfamily (11,12). Importin-β is a highly versatile molecule that is able to transport a variety of cargoes by binding them directly or through an adaptor protein (13–15). Importin-β:cargo complexes form in the cytosol and then cross the nuclear pore and enter the nucleus, where the complexes dissociate upon binding of the small GTPase Ran, in its GTP-bound form (16–18). The Importin-β:RanGTP complex shuttles back to the cytoplasm, where GTP hydrolysis is triggered and RanGDP is released, closing the cycle (19,20). Its unusual structural characteristics give Importin-β great flexibility, enabling it to undergo the rapid structural transitions involved in transport (21–26). Importin-β is an α-solenoid protein composed of 19 structurally conserved HEAT (Huntingtin, elongation factor 3, a subunit of protein phosphatase 2A, TOR (target of rapamycin 1)) repeats (27). Each HEAT repeat comprises two antiparallel α-helices connected by a loop (Fig. 1 *A*). The N-terminal A-helix is exposed at the outside, whereas the B-helix is located at the inner surface. This consecutive arrangement results in the overall superhelical shape of Importin-β (22,25,28–30). Solenoid proteins exhibit only very few contacts between residues distant in primary sequence, conveying a remarkable flexibility (25,31,32). The central HEAT repeats of Importin-β are more flexible compared with the remaining HEATs, resulting in an N-terminal and a C-terminal arch connected by hinge regions (16).

Both cargoes and RanGTP bind to the concave inner surface of Importin-β, although in different regions (24). The binding site for cargoes is located in the central HEAT repeats (28). The adaptor proteins Importin-α and Snurportin1, which bridge the interaction between Importin-β and

Submitted February 3, 2015, and accepted for publication June 8, 2015.

*Correspondence: hgrubmu@gwdg.de or hneumann@uni-goettingen.de

Kangkan Halder and Nicole Dölker contributed equally to this work.

Helmut Grubmüller and Heinz Neumann contributed equally to this work.

Nicole Dölker's present address is Structural Computational Biology Group, Spanish National Cancer Research Centre (CNIO), Madrid, Spain.

Editor: Scott Feller.

0006-3495/15/07/0277/10 $2.00

http://dx.doi.org/10.1016/j.bpj.2015.06.014

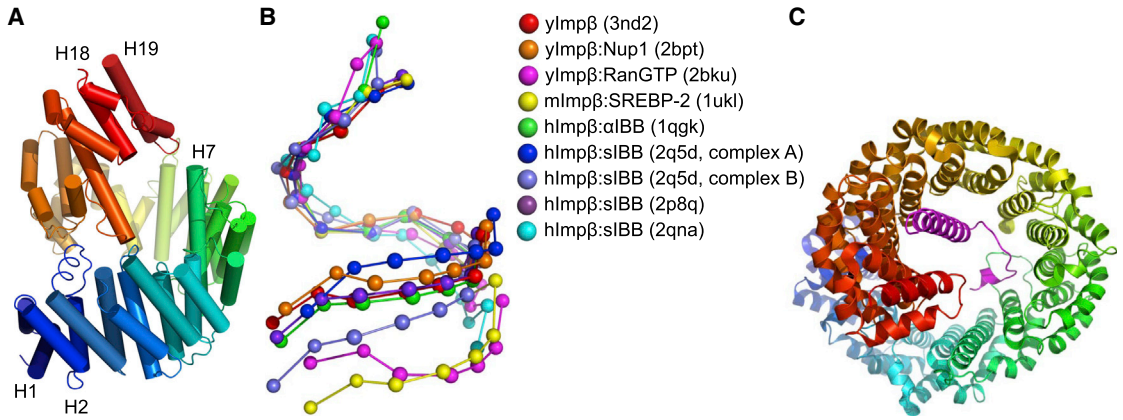

FIGURE 1 Conformations of Importin-β. (*A*) Structure of Importin-β, shown in cartoon representation with α-helices represented by cylinders, colored by HEAT repeats from the N-terminus (*blue*) to the C-terminus (*red*). (*B*) Conformational variety of crystal structures of Importin-β (PDB IDs are given in the legend). The centers of mass of the HEAT repeats are shown. Importin-β from different organisms (yImpβ: yeast; mImpβ: mouse; hImpβ: human). (*C*) Importin-β bound to the sIBB domain (*magenta*). To see this figure in color, go online.

cargoes, contain an α-helical Importin-β binding (IBB) domain that is enclosed by the C-terminal HEAT repeats (13,22,30,33–36). RanGTP attaches to the N-terminally located CRIME (for Crm1, Importin-β, etc.) domain (16,37,38), which is the most conserved sequence motif among nuclear transport receptors (11).

To mediate transport across the nuclear envelope, Importin-β has to interact with hydrophobic patches on FG nucleoporins of the NPC (5,39). The phenylalanine side chains can interact with the outer convex surface of Importin-β, where they insert into hydrophobic clefts between adjacent HEAT repeats (40–42), allowing the complexes to cross the nuclear envelope efficiently. The key factor for successful nuclear transport is the high hydrophobicity of the outer surface of nuclear transport receptors (9).

Structural studies on Importin-β have produced a disparate image of its conformational flexibility. Small-angle x-ray scattering (SAXS) studies and molecular-dynamics (MD) simulations suggested a rather extended conformation of free Importin-β in solution (31,32,43), whereas most crystal structures, with some conflicting exceptions, displayed more compact conformations (Fig. 1 *B*). No clear correlation has been observed between the binding mode of the interacting proteins and the conformation of the superhelix, and MD simulations uniformly predicted large differences in the flexibility of the different Importin-β complexes (32).

As a possible explanation for these discrepancies, we speculated that Importin-β displays environmentally induced plasticity. To test the possible impact of solvent polarity on the conformation of Importin-β, we carried out extended MD simulations of free Importin-β and of Importin-β in complex with the IBB domains of Importin-α (αIBB) or Snurportin1 (sIBB) in solvents of different polarity. In the simulations, free Importin-β and both IBB domain complexes adopted a significantly more compact structure in methanol than in aqueous solution. We subsequently confirmed this prediction by biophysical experiments, which showed an increased energy transfer between two fluorophores installed on Importin-β in more hydrophobic solvents. These conformational changes may play a role in the nuclear import cycle.

MATERIALS AND METHODS

MD simulations

For the MD simulations, the crystal structures of the molecular complexes of Importin-β bound to the IBB domains of Importin-α (PDB ID: 1QGK) (20) and Snurportin1 (32) (PDB ID: 2P8Q) were used. The protonation states of titratable groups were determined using WHAT IF (44). For the simulations of free Importin-β, the IBB domain was removed from the crystal structures. The structures were placed in cubic boxes of sufficient size, such that the minimal distance between the protein and the box edges was at least 2 nm. Subsequently, the structures were solvated with either water or methanol, resulting in an average number of ~76,800 water and 32,500 methanol molecules, respectively. Na^+ and Cl^- ions were added at a 0.15 M concentration.

All MD simulations were carried out with the GROMACS program package (45) (CVS version from 2007-07-20 and version 4.0) using the OPLS-AA force field (46) and the SPC water model (47) with 0.15 M Na^+ and Cl^- ions. These parameters were previously used for simulations of α-solenoid proteins and were shown to give reliable results (31,32,48,49).

For the simulations in methanol, a box with 1728 methanol molecules, preequilibrated with the OPLS force field at 298 K and 1 bar, was used (50). Radii of gyration were calculated with the GROMACS tool *g_gyrate*. SAXS curves were simulated using the FOXS program (51,52). All structural figures were created with Pymol (53). For details regarding the simulation parameters and the calculation of the statistical uncertainty, see Supporting Materials and Methods in the Supporting Material.

Protein expression and labeling

The construct *hs*Impβ-sfGFP-His_6 (human Importin-β fused to superfolder green fluorescent protein (sfGFP) with a C-terminal hexa-histidine tag) was cloned into pCDFDuet-1 (Merck Millipore), and amber codons introduced by site-directed mutagenesis to create *hs*Imp$\beta^{Q220TAG}$-sfGFP-His_6 and *hs*Imp$\beta^{Y255TAG}$-sfGFP-His_6. Proteins were expressed in *E. coli* BL21(DE3) transformed with plasmids to encode target proteins and *Mj*CNPheRS/$tRNA_{CUA}$, and purified according to standard protocols (Supporting Materials and Methods). Purified proteins were labeled with

dibenzocyclooctyne-conjugated (DBCO) dyes in ~20-fold molar excess for 2 h in the dark, followed by native PAGE purification and electroelution. Native PAGE purification was necessary to remove remaining free fluorophore and a truncated form of *hs*Impβ-sfGFP (see Fig. 4 *B*, lower band in lane 2). The extent of labeling of *hs*Impβ-sfGFP Q220AzF-Fl-545 and *hs*Impβ-sfGFP Y255AzF-Fl-545 was qualitatively assessed by in-gel fluorescence, which showed a single dual-fluorophore-labeled band after the final purification step (Fig. S7). Samples were supplemented with glycerol (5–10%) as a cryoprotectant and snap-frozen in liquid nitrogen.

Förster resonance energy transfer measurements

Fluorescence scans were performed on a Fluoromax-4 (Horiba Scientific) with a 10 × 2 mm fluorescence cuvette (104002F-10-40; Hellma Analytics), with the following settings: temperature = 20°C, band width = 3/3 nm, resolution = 1 nm, and integration time = 0.1 s. The emission spectra were normalized to maximum = 1 and minimum = 0. The relative Förster resonance energy transfer (FRET) efficiency (see Fig. 5, *B* and *C*) was calculated as $E_{FRET} = I_A/(I_A + I_D)$, where I_D and I_A are the fluorescence intensities at donor emission maximum (508 nm) and acceptor emission maximum (575 nm), respectively, from a single emission scan after excitation of the donor (470 nm).

RESULTS

Previous structural studies have focused on the influence of cargo binding on the conformation of Importin-β. However, it is possible that the observed structural discrepancies are the result of the different solvents used in crystallization. These solvents differed substantially in polarity, mainly due to the amount of polyethylene glycol (PEG) present in the solution (Table S2) (22,30,33,36). This behavior may be relevant in vivo since Importin-β experiences a more hydrophobic environment in the channel of the NPC.

Structure and dynamics of Importin-β in aqueous solution

To test this hypothesis, we chose to use x-ray crystal structures of Importin-β bound to the sIBB or αIBB domain and of free Importin-β, after in silico removal of the IBB domain, as representative examples to carry out unbiased all-atom MD simulations in explicit solvent (for an overview of the simulations, see Table S1).

In all simulations using Importin-β:sIBB (PDB ID: 2P8Q) as the starting point (Fig. 1 *C*), Importin-β underwent rapid structural changes (Fig. 2 *A*, *blue lines*). Within 100 ns, the complex opened noticeably, expanding the radius of gyration (R_g) from 3.17 to 3.45 ± 0.01 nm (calculated from the last 20 ns of the trajectories) (Table 1; for the estimation of errors, see Supporting Materials and Methods). Therefore, the closed conformation of the Importin-β:sIBB complex is not stable during MD simulations in aqueous solution. Instead, Importin-β:sIBB exhibits a large conformational plasticity, especially in the N-terminal arch. However, all representative structures showed a larger opening of the superhelix than the crystal structure (see Fig. S1). Similar results were obtained with αIBB-bound Importin-β (PDB ID: 2QGK) (22) (Fig. 2 *A*, *red lines*).

The conformational changes of Importin-β in aqueous solution are reflected in the backbone root mean-square deviation (RMSD) with respect to the closed crystal structure (see Fig. S2). In each frame of the trajectory, all backbone atoms of the complete scaffold of Importin-β were aligned to the closed crystal structure. Subsequently, the RMSD was calculated separately for each HEAT repeat of the aligned structures. For the sIBB complex (Fig. S2 *A*), the inner groove of Importin-β (HEAT repeats H8–H12) was the most rigid, and the N- and C-termini showed higher flexibility. This pattern of flexibility is in agreement with previous studies that analyzed the flexibility of Importin-β and found that it was mainly determined by movements around two major hinges at H4-5 and H14-15 (32). For the αIBB complex, the pattern was slightly different (Fig. S2 *B*). In three out of four simulations the pattern was similar to that of the sIBB complex, whereas in one simulation the N-terminus was drastically distorted.

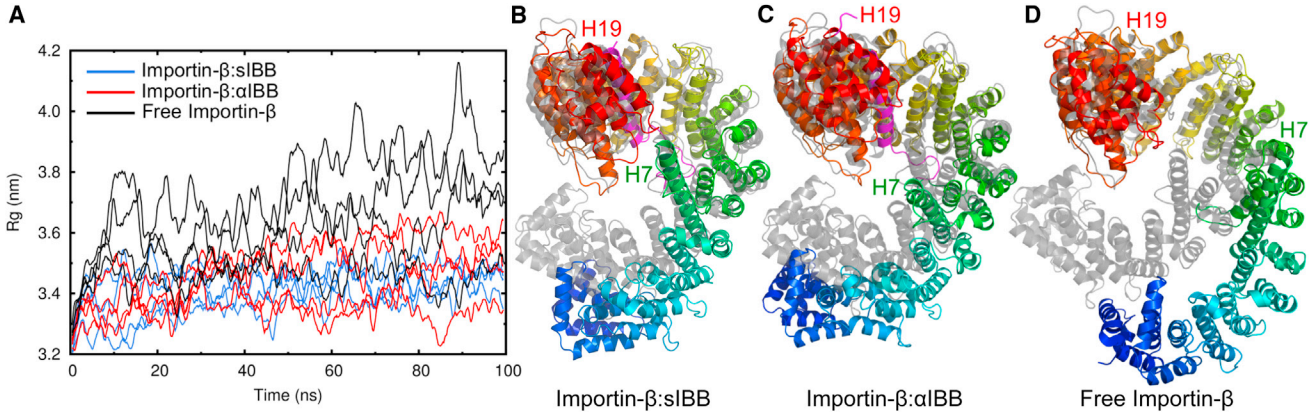

FIGURE 2 Importin-β in aqueous solution. (*A*) Running average of the R_g of Importin-β complexed with the sIBB domain (*blue*) or the αIBB domain (*red*) compared with free Importin-β (*black*). (*B–D*) Snapshots after 100 ns of MD simulation of the sIBB complex (*B*), αIBB complex (*C*), and free Importin-β (*D*) compared with the corresponding closed crystal structures in gray. For clarity, the structures were aligned at the less variable HEAT repeats 11–19. To see this figure in color, go online.

TABLE 1 Radius of gyration of Importin-β

Importin-β in Complex with	R_g (nm) Crystal Structure	R_g (nm) Simulation in Water	R_g (nm) Simulation in Methanol
sIBB	3.17	3.45 (0.01)	3.32 (0.01)
αIBB	3.16	3.48 (0.06)	3.37 (0.01)
—	3.17/3.16[a]	3.71 (0.08)	3.50 (0.03)

The R_g of Importin-β in water was averaged over all independent simulations. Only the last 20 ns of each simulation were included in the calculation. The estimated statistical uncertainty is given in parentheses (see Supporting Materials and Methods).

[a]The starting structure of four of the five simulations of free Importin-β in water was obtained from PDB 2P8Q after removal of sIBB, and one was obtained from PDB 2QGK after removal of αIBB.

The predominant flexibility of the N-terminus of Importin-β also becomes evident from a comparison of snapshots from the trajectories with the closed crystal structure (Fig. 2, *B* and *C*). In all simulations, the IBB domain remained bound to Importin-β. Whereas the conformation of the α-helical part of the IBB domain was largely unchanged (with RMSD values of 0.1–0.3 nm, compared with the crystal structure), the N-terminal loop stretched slightly to adapt to the more open conformation of Importin-β, reaching RMSD values of up to 0.5 nm.

These MD simulations indicate that in water, at physiological salt concentration, the Importin-β:IBB domain complexes adopt markedly more extended conformations compared with the crystal structures. In the simulations, the C-terminal arch was closed and tightly wrapped around the cargo, whereas the N-terminus was quite flexible. Experimental evidence for such an open conformation of Importin-β in solution comes from SAXS studies on the ligand-free state (25). On the basis of these data, it was proposed that free yeast Importin-β in solution has an extended R_g of 3.9 nm.

To check our MD simulations against the SAXS experiments, and to understand the influence of cargo binding on the conformation and flexibility of Importin-β, we carried out simulations of human Importin-β from which the bound IBB domain had been removed (Fig. 2 *A*, *black lines*). In our simulations, free Importin-β clearly showed a more pronounced opening and a larger flexibility than the IBB domain complexes (Fig. 2 *D*): during 100 ns of simulation, R_g values of up to 4.2 nm were reached, with an average R_g of 3.71 $\pm$ 0.08 nm (Fig. 2 *D*; Table 1). These conformational changes occurred along the entire superhelix of Importin-β, with the largest fluctuations being observed within the N- and C-terminal HEAT repeats (Fig. S2 *C*). We calculated theoretical SAXS curves from snapshots from the last 50 ns of all simulations. The resulting averaged scattering profile correctly reproduced the features observed in SAXS studies of yeast Importin-β (KAP95), including the characteristic shoulder at $q \approx 1\ nm^{-1}$ (Fig. S3) (25,43).

To summarize, in all of the MD simulations in aqueous solution with a physiological ion concentration, all closed crystal conformations of Importin-β turned out to be unstable and quickly adopted a more relaxed and open conformation. Even though the IBB domain complexes were found to be more compact than free Importin-β, a noticeable opening of the Importin-β superhelix was also seen in both of the Importin-β:IBB domain complexes under study.

Sensitivity of Importin-β to solvent polarity

The observation that the closed conformations of free Importin-β and the Importin-β:IBB domain complexes opened up during MD simulations in water led us to ask whether the abundance of compact crystal structures may be due to the crystallization conditions. The good agreement between the simulations and SAXS experiments supports this idea. In fact, most crystals of Importin-β were obtained using PEG, which facilitates protein crystallization by lowering the polarity of the medium, as a precipitant (Table S2). The crystals of the open conformation of the Importin-β:sIBB complex, in contrast, were obtained in the absence of PEG (30).

To test whether less polar solvents can indeed induce closed structures of Importin-β, we carried out MD simulations of cargo-free and cargo-bound Importin-β in methanol as a hydrophobic mimic of both the PEG solution and the interior of the nuclear pore. The simulations were started from three different conformations of the sIBB complex (Fig. S4, *A* and *B*) or the αIBB complex (Fig. S4, *C* and *D*) using crystal structures or, as controls, open conformations extracted from previous simulations in water. Simulations of free Importin-β were started from the closed structure and from an open conformation with an R_g of 3.9 nm (Fig. S4 *E*). Contrary to what was observed in aqueous solution, the closed crystal structure of the Importin-β:sIBB complex opened only slightly in methanol (Fig. 3 *A*, *black line*). Strikingly, all simulations of open conformations showed a marked decrease of the R_g of the complex, reaching average values between 3.32 $\pm$ 0.01 nm (Importin-β:sIBB) and 3.50 $\pm$ 0.03 nm (free Importin-β), thus indicating a pronounced shift in the conformational equilibrium (Table 1). In all simulations starting from an open conformation with little distortion of individual HEAT repeats, the N-terminus closed spontaneously within 10–20 ns (Fig. 3 *A*, *cyan lines*). This conformational change brought the termini of Importin-β into contact, forming a closed ring, which then remained stable during the rest of the simulation (Fig. 3 *B*). The final conformation was even more compact than in the crystal structure (Fig. S4 *F*).

In cases where the starting structure displayed more local distortions of individual HEAT repeats, the conformational rearrangement was slower (Fig. 3 *A*, *blue lines*). Within 100 ns, a noticeable decrease in R_g was observed, but a conformation with stable contacts between the N- and C-terminal regions was not reached (Fig. 3 *C*). However, an overall compaction and a transient ring closure of Importin-β were also seen in these cases.

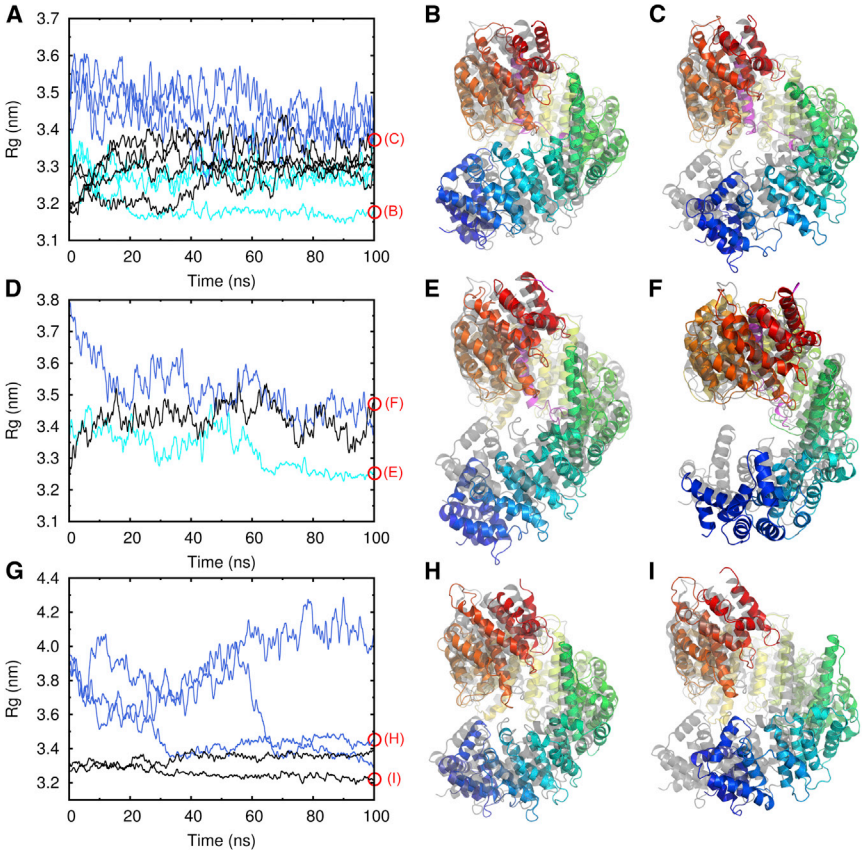

FIGURE 3 Importin-β in methanol. (*A*) Running average of the R_g of the Importin-β:sIBB complex. Simulations started from the closed conformation (*black*) and from open conformations with little deformation of individual HEAT repeats (*cyan*) and stronger deformation (*blue*). (*B* and *C*) Snapshots after 100 ns of simulations compared with the crystal structures (in *gray*). (*D*) R_g of the Importin-β:αIBB complex. (*E* and *F*) Snapshots after 100 ns of simulation. (*G*) Running average of the R_g of free Importin-β. (*H* and *I*) Snapshots after 100 ns of simulation time. Red circles indicate where the displayed snapshots were taken. To see this figure in color, go online.

The Importin-β:αIBB and sIBB complexes exhibited similar R_g values in methanol, with final values reaching 3.25–3.5 nm (Fig. 3 *D*). However, the corresponding structures showed a larger conformational variety (Fig. 3, *E* and *F*). The contacts between the N- and C-terminal HEAT repeats were less stable, as reflected by the larger RMSD (0.5–0.8 nm) compared with the crystal structure (Fig. S4 *G*).

For uncomplexed Importin-β, the less polar solvent methanol also stabilized a compact structure of the superhelix. Even after removal of the IBB domain, the structure remained rather stable (Fig. 3 *G*, *black lines*, and *H*). Two of the three simulations of Importin-β that started from a completely open conformation, with no sequence distal contacts between HEAT repeats, completed closure within 40 and 70 ns (Fig. 3 *D*, *blue lines*). Although contacts between the N- and C-termini were formed, a certain conformational heterogeneity within the ensemble of closed structures remained (Figs. 3, *H* and *I*, and S4 *H*). The deviations from the crystal structure are due to a lack of stabilization of the C-terminus and the central arch of Importin-β by the IBB domain.

The simulations show that despite their conformational differences, free Importin-β and both of the IBB domain complexes adopt a markedly more compact structure in methanol than in aqueous solution. This reaction to the polarity of the environment is therefore an intrinsic property of Importin-β. The large rearrangements, which lead to closure of the Importin-β superhelix, take place very rapidly, on a timescale of ~100 ns.

A major conformational change of a large and highly flexible system such as Importin-β is a stochastic process that requires the crossing of numerous energetic barriers. The observed differences between the trajectories corresponding to independent simulations of the same system are thus not surprising. Nevertheless, from the simulations alone we cannot exclude the possibility, however remote, that the observed trends could be artifacts stemming from insufficient convergence of the simulations. We therefore addressed the significance of the results from the simulations by conducting experiments.

Increased energy transfer in dual-fluorophore-labeled Importin-β in hydrophobic solvents

We aimed to test the above theoretical observations biochemically by assessing the conformational plasticity of Importin-β in response to differences in the hydrophobicity of the environment. To this end, we produced dual-fluorophore-labeled Importin-β to observe shape changes by measuring the FRET efficiencies. Site-specific coupling of fluorophores to Importin-β is impeded by the presence of

more than 20 cysteine residues in the natural sequence, precluding the use of thiol chemistry. Therefore, we genetically fused sfGFP (54) as the donor fluorophore to the C-terminal end of *hs*Importin-β (*hs*Impβ-sfGFP). The fluorescence properties of sfGFP are unaffected in the fusion construct (Fig. S5). To introduce the acceptor fluorophore, we used genetic-code expansion to install amino acids with side chains containing bioorthogonal reactive functional groups at structurally permissive sites. These amino acids are activated by evolved aminoacyl-tRNA synthetases and incorporated in response to amber (UAG) codons by corresponding cognate tRNAs. We chose the surface-exposed residues Gln-220 and Tyr-255 for incorporation of *p*-azido-L-phenylalanine (AzF) using the evolved *Mj*CNPheRS/$tRNA_{CUA}$ pair (55) (Fig. 4 *A*). Full-length protein was produced only when AzF was supplied with the growth medium (Fig. S6), confirming the successful incorporation of the amino acid in response to the amber codon. We used the azide group to site-specifically conjugate the fluorophore DBCO-Fl-545 in a bioorthogonal strain promoted azide-alkyne coupling (SPAAC) (Figs. 4 *B* and S7). In fluorescence emission scans ($\lambda_{ex.} = 470$ nm) of *hs*Impβ-sfGFP Q220AzF-Fl-545, we observed an additional intensity around 575 nm, which depended on the presence of the acceptor fluorophore and therefore may indicate the presence of intramolecular FRET (Fig. S8). Treating the labeled protein with Proteinase K removed this additional intensity at ~575 nm (Fig. S9 *A*). When the unlabeled *hs*Impβ-sfGFP was supplemented with free DBCO-Fl-545 dye and treated with Proteinase K, no such change at ~575 nm was observed (Fig. S9 *B*). Hence, we conclude that a small amount of FRET occurs between sfGFP and Fl-545 in *hs*Impβ-sfGFP Q220AzF-Fl-545, which may be used to report on changes in the protein's conformation in response to the surrounding medium. As a functional test for correct folding, we incubated permeabilized HeLa cells with labeled *hs*Impβ-sfGFP proteins. As shown in Fig. S10, the protein was detected in the nucleus and also at the nuclear envelope, indicating physiological interactions with components of the nuclear transport machinery.

First, we investigated the FRET efficiency in the presence of increasing concentrations of methanol, similar to the conditions used in the simulation experiments (Fig. S11). Indeed, we observed an increase in FRET with increasing methanol concentration, indicating that *hs*Importin-β contracts in hydrophobic environments. Next, we tested the impact of the addition of PEG of various molecular weights on the FRET efficiency in *hs*Impβ-sfGFP Q220AzF-Fl-545 (Fig. 5 *A*). PEG creates a more crowded and hydrophobic environment, an effect that escalates with increasing chain length. At 50% (w/v) PEG 200 the fluorescence intensity at 575 nm of *hs*Impβ-sfGFP Q220AzF-Fl-545 rose slightly, whereas higher-molecular-weight PEG at the same concentration showed increasingly stronger effects. Titrating the concentration of PEG 200, PEG 1500, and PEG 4000 over

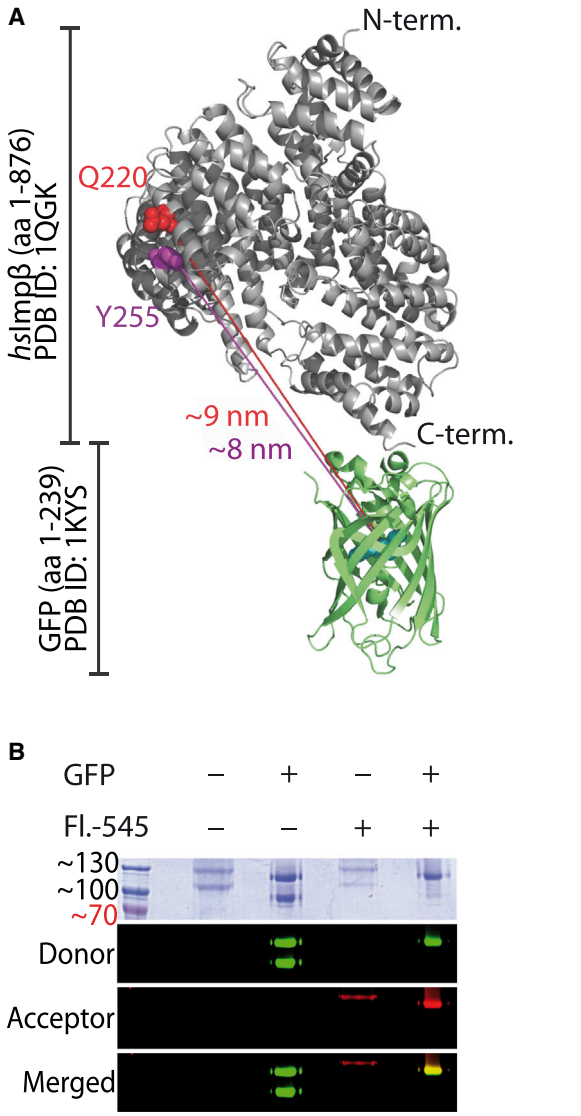

FIGURE 4 Dual-fluorophore labeling of *hs*Importin-β. (*A*) Cartoon model of *hs*Importin-β showing the positions of AzF incorporation and their approximate distances to the sfGFP fluorophore. The figure was created using Pymol v0.99 and PDB entries 1QGK and 1KYS. (*B*) Importin proteins with or without genetically fused sfGFP-tag were purified from *E. coli* and labeled with DBCO-Fl.-545 where indicated. Fluorescence was analyzed using a Typhoon phosphoimager. To see this figure in color, go online.

the range of 0–50% (w/v) revealed that relative FRET efficiency increased with PEG molecular weight and concentration (Figs. 5, *B* and *C*, and S12). The increase in acceptor fluorescence is indeed a result of enhanced energy transfer because a mixture of *hs*Impβ-sfGFP and DBCO-Fl-545 did not react to the addition of PEG in this manner (Fig. S13). This effect was not a simple result of molecular crowding, since Ficoll-70 (molecular weight 70,000), which induces crowding but is not hydrophobic, did not show a similar effect on the fluorescence properties of *hs*Impβ-sfGFP Q220AzF-Fl-545 (Fig. S14). This compaction was

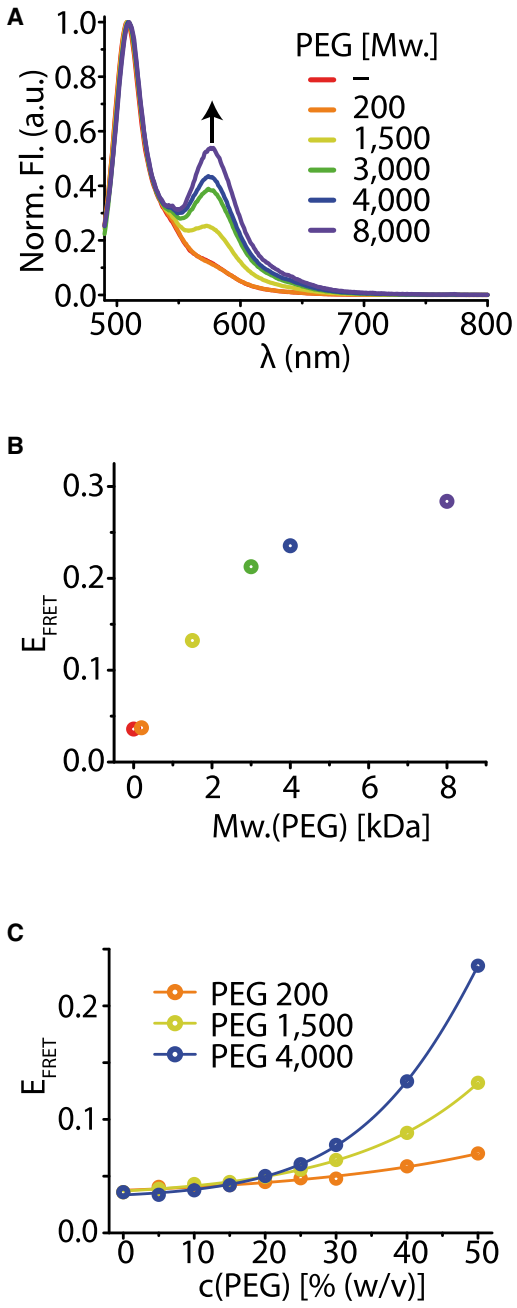

FIGURE 5 *hs*Impβ-sfGFP Q220AzF-Fl-545 shows increased FRET in the presence of PEG. (*A*) Addition of 50% (w/v) PEG of various molecular weights leads to an increase in fluorescence emission at 575 nm. (*B*) The relative FRET efficiency of *hs*Impβ-sfGFP Q220AzF-Fl-545 calculated from the emission spectra in (*A*). (*C*) Relative FRET efficiency increases with PEG concentration. To see this figure in color, go online.

reversible, as expected for Importin-β exiting the NPC, as demonstrated by stepwise dilution of *hs*Impβ-sfGFP Q220AzF-Fl-545 from 50% PEG solutions (Fig. S15). We obtained similar results using an alternative spectroscopic method when we measured the interaction of the fluorophores by donor fluorescence lifetime instead of energy transfer. Again, increasing concentrations and molecular weights of PEG reduced the donor fluorophore lifetime to a similar degree as observed by FRET (Fig. S16).

These experiments confirm our simulation results showing that Importin-β indeed adopts a more compact conformation in hydrophobic environments.

DISCUSSION

The high intrinsic flexibility of Importin-β has received considerable attention, and it is generally accepted that it is of paramount importance for the fast binding and release of a wide variety of cargoes (21–26). However, previous studies have been centered on the function of conformational changes in cargo binding, and little attention has been paid to their possible role in crossing of the nuclear pore. Recent findings, as well as our simulations, suggest that due to its unique and complex hydrophobic core, Importin-β in solution fluctuates in equilibrium between different conformational states, comprising completely open as well as quite compact conformations of the superhelix (25,31,33). Cargo binding shifts the equilibrium toward more closed conformations by selecting rather strained conformers of Importin-β from this large pool of different conformations, with the corresponding entropy changes being crucial for the overall thermodynamics of the system. Similar observations were made for the exportin Crm1, which cooperatively adopts more compact conformations upon binding RanGTP and cargo (56). However, available structural models of Importin-β do not fully support this perception. Whereas models built from SAXS experiments show free Importin-β in rather open conformations, x-ray crystallography has yielded predominantly closed, compact structures of both free and cargo-bound Importin-β.

In our MD simulations, we observed that binding of the IBB domain of the adaptor proteins Importin-α and Snurportin1 to the inner surface of Importin-β indeed stabilized more compact conformations of the superhelix, in line with the current model. However, in our simulations, the IBB domain stabilized only the C-terminal arch of Importin-β (HEAT repeats 12–19), which is in direct contact with the helical part of the IBB domain. Other domains of the molecule underwent large conformational changes, adopting an open conformation. This flexibility may have functional implications, e.g., for RanGTP binding and unbinding.

Strikingly, in all simulations with a more hydrophobic solvent, such as methanol, the structure of Importin-β favored closed conformations. Rapid closure was seen in all simulations of Importin-β, whether or not it was bound to an IBB domain. Further, the superhelix adopted a conformation that largely resembled the closed conformations seen in most Importin-β crystal structures. This unusually strong influence of environment polarity on Importin-β structure is corroborated by a clear correlation between the crystallization conditions and the observed Importin-β

conformation. In fact, most crystals containing closed conformations were obtained in solutions of high PEG concentrations with a markedly decreased polarity, whereas the crystal structure obtained from a PEG-free solution showed a much more open conformation (Table S2). Similar conformational plasticity of Importin-β in response to changes in the polarity of the solvent (by addition of different types of alcohols) was observed in a recent study (57).

Overall, our biochemical and theoretical studies suggest that the closed structures of cargo-bound Importin-β do not represent the predominant conformation in the cytoplasm, but rather conformations of Importin-β in a less polar environment.

This finding suggests an unexpected functional role of the environment during nucleo-cytoplasmic transport, where Importin-β is subject to changes in the surrounding medium. In the cytoplasm or nucleoplasm, it is exposed to aqueous solvent, whereas inside the central channel of the NPC, the high concentration of hydrophobic FG repeat peptides reduces the polarity of the solvent (4) in a manner similar to that observed for PEG. We therefore assume that Importin-β also adopts a more compact conformation upon entering the nuclear pore. It is tempting to speculate that the transitions between open and closed conformations correspond to the varying requirements for the stability of Importin-β complexes with cargo molecules during different stages of the transport process (Fig. 6). In the cytoplasm, Importin-β binds cargoes at its concave inner surface. An open conformation of the superhelix would make the binding sites more accessible and facilitate cargo recognition. During the passage through the nuclear pore, the inside of the superhelix needs to be protected against interactions with other molecules present in the channel to prevent dissociation of the cargo-transporter complex. Closed conformations would prevent the complex from dissociating during passage. After it is imported into the nucleus, the IBB domain is displaced from Importin-β by RanGTP, which would be facilitated by an opening of the complex in the polar environment of the nucleoplasm. Such environment-sensitive conformational plasticity may in fact be quite a general mechanism to modulate or control protein function in response to environmental changes. Such changes may be due to molecular crowding, solute concentration changes, or molecular transitions between different intracellular compartments.

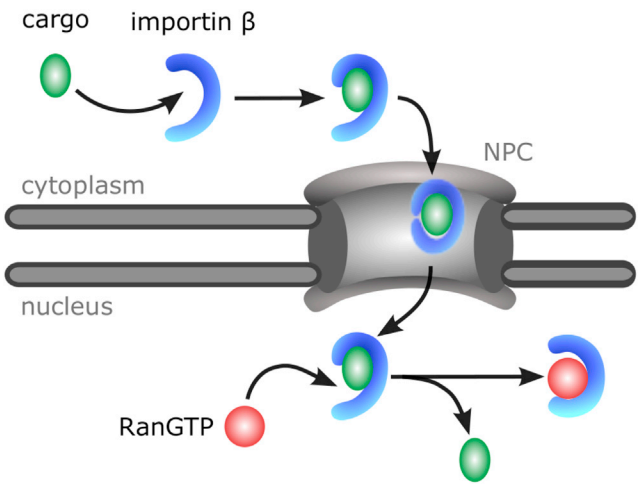

FIGURE 6 Proposed model for Importin-β-dependent transport. In the aqueous solution of the cytoplasm, Importin-β adopts predominantly open conformations, rendering its inner surface more accessible to ligand binding (*upper part*). When cargo-bound Importin-β enters the NPC, contact with the hydrophobic permeability barrier leads to closure of the Importin-β superhelix, thus preventing complex dissociation during passage (*central part*). After the complex exits from the pore, the N-terminus opens up again, rendering Importin-β accessible to RanGTP binding (*lower part*). To see this figure in color, go online.

SUPPORTING MATERIAL

Supporting Materials and Methods, 16 figures, and two tables are available at http://www.biophysj.org/biophysj/supplemental/S0006-3495(15)00596-2.

AUTHOR CONTRIBUTIONS

K.H. produced recombinant proteins. K.H. and Q.V. performed FRET experiments. I.B. carried out fluorescence microscopy experiments. N.D. performed MD simulations. I.G. contributed analytic tools. K.H., N.D., H.G., and H.N. wrote the manuscript. All authors designed experiments, analyzed data, and commented on the manuscript.

ACKNOWLEDGMENTS

We thank Clement Blanchet, Daniel Wohlwend, Thomas Monecke, and Ulrich Zachariae for helpful discussions, and Thomas Monecke for carefully reading the manuscript.

This work was supported by grants from the Human Frontiers Science Program (grant RGP53/2004), the Deutsche Forschungsgemeinschaft (GR 2079/4-1 to H.G., Ke660/14-1 to R.K., and SFB860 to J.E., R.F., and H.N.), the Emmy-Noether Programme of the Deutsche Forschungsgemeinschaft, the Free Floater Programme of the University of Göttingen (to H.N.), and the Cluster of Excellence and DFG Research Center Nanoscale Microscopy and Molecular Physiology of the Brain (to J.E., H.G., and H.N.).

SUPPORTING CITATIONS

References (58–60) appear in the Supporting Material.

REFERENCES

1. Lim, R. Y. H., and B. Fahrenkrog. 2006. The nuclear pore complex up close. *Curr. Opin. Cell Biol.* 18:342–347.
2. Keminer, O., and R. Peters. 1999. Permeability of single nuclear pores. *Biophys. J.* 77:217–228.
3. Ma, J., A. Goryaynov, …, W. Yang. 2012. Self-regulated viscous channel in the nuclear pore complex. *Proc. Natl. Acad. Sci. USA.* 109:7326–7331.

4. Kramer, A., I. Liashkovich, …, V. Shahin. 2008. Atomic force microscopy visualises a hydrophobic meshwork in the central channel of the nuclear pore. *Pflugers Arch.* 456:155–162.
5. Wälde, S., and R. H. Kehlenbach. 2010. The Part and the Whole: functions of nucleoporins in nucleocytoplasmic transport. *Trends Cell Biol.* 20:461–469.
6. Chook, Y. M., and K. E. Süel. 2011. Nuclear import by karyopherin-βs: recognition and inhibition. *Biochim. Biophys. Acta.* 1813:1593–1606.
7. Cook, A. G., and E. Conti. 2010. Nuclear export complexes in the frame. *Curr. Opin. Struct. Biol.* 20:247–252.
8. Xu, D., A. Farmer, and Y. M. Chook. 2010. Recognition of nuclear targeting signals by Karyopherin-β proteins. *Curr. Opin. Struct. Biol.* 20:782–790.
9. Naim, B., D. Zbaida, …, Z. Reich. 2009. Cargo surface hydrophobicity is sufficient to overcome the nuclear pore complex selectivity barrier. *EMBO J.* 28:2697–2705.
10. Wang, R., and M. G. Brattain. 2007. The maximal size of protein to diffuse through the nuclear pore is larger than 60kDa. *FEBS Lett.* 581:3164–3170.
11. Görlich, D., M. Dabrowski, …, E. Izaurralde. 1997. A novel class of RanGTP binding proteins. *J. Cell Biol.* 138:65–80.
12. Radu, A., G. Blobel, and M. S. Moore. 1995. Identification of a protein complex that is required for nuclear protein import and mediates docking of import substrate to distinct nucleoporins. *Proc. Natl. Acad. Sci. USA.* 92:1769–1773.
13. Huber, J., U. Cronshagen, …, R. Lührmann. 1998. Snurportin1, an m3G-cap-specific nuclear import receptor with a novel domain structure. *EMBO J.* 17:4114–4126.
14. Jäkel, S., and D. Görlich. 1998. Importin beta, transportin, RanBP5 and RanBP7 mediate nuclear import of ribosomal proteins in mammalian cells. *EMBO J.* 17:4491–4502.
15. Palmeri, D., and M. H. Malim. 1999. Importin beta can mediate the nuclear import of an arginine-rich nuclear localization signal in the absence of importin alpha. *Mol. Cell. Biol.* 19:1218–1225.
16. Lee, S. J., Y. Matsuura, …, M. Stewart. 2005. Structural basis for nuclear import complex dissociation by RanGTP. *Nature.* 435:693–696.
17. Sun, C., G. Fu, …, S. M. Musser. 2013. Choreography of importin-α/CAS complex assembly and disassembly at nuclear pores. *Proc. Natl. Acad. Sci. USA.* 110:E1584–E1593.
18. Sun, C., W. Yang, …, S. M. Musser. 2008. Single-molecule measurements of importin alpha/cargo complex dissociation at the nuclear pore. *Proc. Natl. Acad. Sci. USA.* 105:8613–8618.
19. Sorokin, A. V., E. R. Kim, and L. P. Ovchinnikov. 2007. Nucleocytoplasmic transport of proteins. *Biochemistry Mosc.* 72:1439–1457.
20. Stewart, M. 2007. Molecular mechanism of the nuclear protein import cycle. *Nat. Rev. Mol. Cell Biol.* 8:195–208.
21. Cingolani, G., H. A. Lashuel, …, C. W. Müller. 2000. Nuclear import factors importin alpha and importin beta undergo mutually induced conformational changes upon association. *FEBS Lett.* 484:291–298.
22. Cingolani, G., C. Petosa, …, C. W. Müller. 1999. Structure of importin-beta bound to the IBB domain of importin-alpha. *Nature.* 399:221–229.
23. Conti, E., C. W. Müller, and M. Stewart. 2006. Karyopherin flexibility in nucleocytoplasmic transport. *Curr. Opin. Struct. Biol.* 16:237–244.
24. Cook, A., F. Bono, …, E. Conti. 2007. Structural biology of nucleocytoplasmic transport. *Annu. Rev. Biochem.* 76:647–671.
25. Forwood, J. K., A. Lange, U. Zachariae, M. Marfori, C. Preast, H. Grubmüller, M. Stewart, A. H. Corbett, and B. Kobe. 2010. Quantitative structural analysis of importin-beta flexibility: paradigm for solenoid protein structures. *Structure.* 18:1171–1183.
26. Lee, S. J., N. Imamoto, …, T. Tsukihara. 2000. The adoption of a twisted structure of importin-beta is essential for the protein-protein interaction required for nuclear transport. *J. Mol. Biol.* 302:251–264.
27. Kobe, B., T. Gleichmann, J. Horne, I. G. Jennings, P. D. Scotney, and T. Teh. 1999. Turn up the HEAT. *Structure.* 7:R91–R97.
28. Lee, S. J., T. Sekimoto, …, Y. Yoneda. 2003. The structure of importin-beta bound to SREBP-2: nuclear import of a transcription factor. *Science.* 302:1571–1575.
29. Liu, S. M., and M. Stewart. 2005. Structural basis for the high-affinity binding of nucleoporin Nup1p to the Saccharomyces cerevisiae importin-beta homologue, Kap95p. *J. Mol. Biol.* 349:515–525.
30. Wohlwend, D., A. Strasser, …, R. Ficner. 2007. Structural basis for RanGTP independent entry of spliceosomal U snRNPs into the nucleus. *J. Mol. Biol.* 374:1129–1138.
31. Kappel, C., U. Zachariae, …, H. Grubmüller. 2010. An unusual hydrophobic core confers extreme flexibility to HEAT repeat proteins. *Biophys. J.* 99:1596–1603.
32. Zachariae, U., and H. Grubmüller. 2008. Importin-beta: structural and dynamic determinants of a molecular spring. *Structure.* 16:906–915.
33. Bhardwaj, A., and G. Cingolani. 2010. Conformational selection in the recognition of the snurportin importin beta binding domain by importin beta. *Biochemistry.* 49:5042–5047.
34. Görlich, D., P. Henklein, …, E. Hartmann. 1996. A 41 amino acid motif in importin-alpha confers binding to importin-beta and hence transit into the nucleus. *EMBO J.* 15:1810–1817.
35. Huber, J., A. Dickmanns, and R. Lührmann. 2002. The importin-beta binding domain of snurportin1 is responsible for the Ran- and energy-independent nuclear import of spliceosomal U snRNPs in vitro. *J. Cell Biol.* 156:467–479.
36. Mitrousis, G., A. S. Olia, …, G. Cingolani. 2008. Molecular basis for the recognition of snurportin 1 by importin beta. *J. Biol. Chem.* 283:7877–7884.
37. Forwood, J. K., T. G. Lonhienne, …, B. Kobe. 2008. Kap95p binding induces the switch loops of RanGDP to adopt the GTP-bound conformation: implications for nuclear import complex assembly dynamics. *J. Mol. Biol.* 383:772–782.
38. Vetter, I. R., A. Arndt, …, A. Wittinghofer. 1999. Structural view of the Ran-Importin beta interaction at 2.3 A resolution. *Cell.* 97: 635–646.
39. Otsuka, S., S. Iwasaka, …, S. H. Yoshimura. 2008. Individual binding pockets of importin-beta for FG-nucleoporins have different binding properties and different sensitivities to RanGTP. *Proc. Natl. Acad. Sci. USA.* 105:16101–16106.
40. Bayliss, R., H. M. Kent, …, M. Stewart. 2000. Crystallization and initial X-ray diffraction characterization of complexes of FxFG nucleoporin repeats with nuclear transport factors. *J. Struct. Biol.* 131:240–247.
41. Bayliss, R., T. Littlewood, and M. Stewart. 2000. Structural basis for the interaction between FxFG nucleoporin repeats and importin-beta in nuclear trafficking. *Cell.* 102:99–108.
42. Isgro, T. A., and K. Schulten. 2005. Binding dynamics of isolated nucleoporin repeat regions to importin-beta. *Structure.* 13:1869–1879.
43. Fukuhara, N., E. Fernandez, …, D. Svergun. 2004. Conformational variability of nucleo-cytoplasmic transport factors. *J. Biol. Chem.* 279:2176–2181.
44. Vriend, G. 1990. WHAT IF: a molecular modeling and drug design program. *J. Mol. Graph.* 8:52–56, 29.
45. Van Der Spoel, D., E. Lindahl, …, H. J. C. Berendsen. 2005. GROMACS: fast, flexible, and free. *J. Comput. Chem.* 26:1701–1718.
46. Kaminski, G. A., R. A. Friesner, …, W. L. Jorgensen. 2001. Evaluation and reparametrization of the OPLS-AA force field for proteins via comparison with accurate quantum chemical calculations on peptides. *J. Phys. Chem. B.* 105:6474–6487.
47. Berendsen, H. J. C., J. P. M. Postma, …, J. Hermans. 1981. Interaction models for water in relation to protein hydration. *In* Intermolecular Forces. B. Pullman, editor. Reidel, Dordrecht, pp. 331–342.
48. Dölker, N., C. E. Blanchet, …, A. Dickmanns. 2013. Structural determinants and mechanism of mammalian CRM1 allostery. *Structure.* 21:1350–1360.

49. Zachariae, U., and H. Grubmüller. 2006. A highly strained nuclear conformation of the exportin Cse1p revealed by molecular dynamics simulations. *Structure.* 14:1469–1478.

50. Böckmann, R. A., and H. Grubmüller. 2004. Multistep binding of divalent cations to phospholipid bilayers: a molecular dynamics study. *Angew. Chem. Int.Engl.* 43:1021–1024.

51. Schneidman-Duhovny, D., M. Hammel, and A. Sali. 2010. FoXS: a web server for rapid computation and fitting of SAXS profiles. *Nucleic Acids Res.* 38:W540–W544.

52. Schneidman-Duhovny, D., M. Hammel, …, A. Sali. 2013. Accurate SAXS profile computation and its assessment by contrast variation experiments. *Biophys. J.* 105:962–974.

53. DeLano, W. L. 2008. The PyMOL Molecular Graphics System. DeLano Scientific, Palo Alto, CA.

54. Pédelacq, J. D., S. Cabantous, …, G. S. Waldo. 2006. Engineering and characterization of a superfolder green fluorescent protein. *Nat. Biotechnol.* 24:79–88.

55. Young, D. D., T. S. Young, …, P. G. Schultz. 2011. An evolved aminoacyl-tRNA synthetase with atypical polysubstrate specificity. *Biochemistry.* 50:1894–1900.

56. Monecke, T., D. Haselbach, …, R. Ficner. 2013. Structural basis for cooperativity of CRM1 export complex formation. *Proc. Natl. Acad. Sci. USA.* 110:960–965.

57. Yoshimura, S. H., M. Kumeta, and K. Takeyasu. 2014. Structural mechanism of nuclear transport mediated by importin β and flexible amphiphilic proteins. *Structure.* 22:1699–1710.

58. Berendsen, H. J. C., J. P. M. Postma, …, J. R. Haak. 1984. Molecular-dynamics with coupling to an external bath. *J. Chem. Phys.* 81:3684–3690.

59. Charneau, P., G. Mirambeau, …, F. Clavel. 1994. HIV-1 reverse transcription. A termination step at the center of the genome. *J. Mol. Biol.* 241:651–662.

60. Hess, B., H. Bekker, …, J. G. E. M. Fraaije. 1997. LINCS: a linear constraint solver for molecular simulations. *J. Comput. Chem.* 18: 1463–1472.

Biophysical Journal

Supporting Material

MD Simulations and FRET Reveal an Environment-Sensitive Conformational Plasticity of Importin-β

Kangkan Halder,[1] Nicole Dölker,[2] Qui Van,[3] Ingo Gregor,[3] Achim Dickmanns,[4] Imke Baade,[5] Ralph H. Kehlenbach,[5] Ralf Ficner,[4] Jörg Enderlein,[3] Helmut Grubmüller,[2,*] and Heinz Neumann[1,*]

[1]Free Floater (Junior) Research Group "Applied Synthetic Biology", Institute for Microbiology and Genetics, Georg-August University Göttingen, Göttingen, Germany; [2]Department of Theoretical and Computational Biophysics, Max-Planck Institute for Biophysical Chemistry, Göttingen, Germany; and [3]Third Institute of Physics-Biophysics, [4]Institute for Microbiology and Genetics, Department of Molecular Structural Biology, and [5]Department of Molecular Biology, Faculty of Medicine, Georg-August University Göttingen, Göttingen, Germany

Supplementary Materials and Methods

Buffers and chemicals: The 4-Azido-L-phenylalanine (AzF, product code: 06162) was purchased from Chem-Impex Inter. Inc. The dibenzocyclooctyne conjugated fluorophore dye (DBCO-Fl-545, product code: CLK-A110-2, currently discontinued from manufacturer) was purchased from Jena Bioscience. The mouse monoclonal anti-His antibody (product code: 27-7410-01), enhanced chemiluminescence (ECL) Prime (product code: RPN2236) and the chemiluminescence Hyperfilm (product code: 28906837) were purchased from GE Healthcare, while the HRP-conjugated anti-Mouse IgG (product code: A4416) was acquired from Sigma Aldrich. The polyethylene glycol (PEG) of different chain lengths (200, 1,500, 3,000, 4,000 and 8,000) were purchased from either Applichem GmbH and/or Sigma Aldrich. The methanol used for titrations is HPLC grade and purchased from VWR Chemicals. Proteinase K (product code: 1092766) was purchased from Boehringer Mannheim GmbH. Vivaspin 500 (product code: Z629367) and Amicon Ultra-15 (product code: UFC903024) centrifugal concentrators were procured from Sigma Aldrich and MerckMillipore, respectively. The D-Tube Dialyzer Midi (product code: 71507-3) and Immobilon-P PVDF Transfer Membrane (product code: IPVH00010) were purchased from MerckMillipore. HisPur Ni-NTA Resin (product code: 88222) was purchased from Thermo Scientific. Other common chemicals and reagents for buffer preparation were purchased from Sigma-Aldrich, Carl Roth GmbH or Applichem. All products were stored, dissolved/ diluted, and used as per manufacturer's protocol.

Plasmids: The human Importin-β (National Center for Biotechnology Information Protein Accession Code : NP_002256.2) and superfolder green fluorescent protein (AGT98536.1) sequences were used to construct the *hs*Impβ-sfGFP-His_6, *hs*Impβ^{Q220TAG}-sfGFP-His_6 and *hs*Impβ^{Y255TAG}-sfGFP-His_6 in the pCDFDuet1 (MerckMillipore) plasmid backbone using the

standard cloning, PCR amplification, restriction enzyme digestion and ligation protocols. The T4 DNA Ligase and Phusion DNA Polymerase were obtained from Thermo Scientific, while the restriction enzymes were obtained from New England Biolabs and Thermo Scientific. The primers for cloning, site directed mutagenesis or sequencing were purchased from Sigma Aldrich as 'purified by desalting'. The plasmids were amplified in *Escherichia coli* DH10B strain in LB medium (10 g Tryptone, 5 g Yeast extract, and 5 g NaCl, in deionized water upto 1 L, pH 7.0) supplemented with Spectinomycin (50 µg/mL final) and purified by peqGOLD Plasmid Miniprep Kit (PeqLab Biotechnologie GmbH). The plasmid integrity was verified by restriction enzyme digestion and DNA sequencing. The complete plasmid sequences of the *hs*Impβ constructs are given below.

Protein Expression and Purification:

***hs*Impβ-sfGFP**: *Escherichia coli* BL21(DE3) (Merck) chemical competent cells were heat-shock transformed with plasmid pCDFDuet1_*hs*Impβ-sfGFP-His_6 and grown overnight in 100 mL of 2YT media (10 g Tryptone, 16 g Yeast extract, and 5 g NaCl, in deionized water upto 1 L, pH 7.0) with Spectinomycin (50 µg/mL) with shaking at 220 rpm at 37°C. Next morning, 1 L 2YT media with Spectinomycin (50 µg/mL) was inoculated at OD_{600} ~0.1 and grown till OD_{600} reached 0.2 – 0.3, when protein expression was induced by adding isopropyl β-D-1-thiogalactopyranoside (IPTG, 500 µM, final) and let grow for another 5 h. The cells were harvested by centrifugation at 4,800 rotations per minute (rpm), snap frozen in liquid nitrogen and stored at -80°C.

The cell pellet was resuspended in ice-cold buffer A (50 mM Tris-Cl, pH 8.0, 200 mM NaCl, 25 mM Imidazole, 1 mM phenylmethanesulfonyl-fluoride and 500 µL of ALP protease inhibitor cocktail) and disrupted by pneumatic cell disintegration using a Microfluidizer 110S (Microfluidics, USA). The cell lysate was cleared by centrifugation at 20,000 rpm, 20 min,

4°C, syringe filtered through 0.2 µm and loaded on a 5 mL Ni^{2+} sepharose HisTrap FF column (GE lifesciences) attached to an Äkta Prime Plus liquid chromatography system (GE lifesciences). The *hs*Impβ-sfGFP was then eluted with buffer B (50 mM Tris-Cl, pH 8.0, 100 mM NaCl, and 200 mM Imidazole) and further purified on a 5 mL HiTrap Q HP column (GE lifesciences), washed with 20 mM Tris-Cl, pH 7.5, 50 mM NaCl and eluted with gradient addition of 20 mM Tris-Cl, pH 7.5, 1 M NaCl. The eluted protein was concentrated using an Amicon Ultra-15 centrifugal filter (30,000 Da cutoff, MerckMillipore).

***hs*Impβ-sfGFP Q220AzF and *hs*Impβ-sfGFP Y255AzF**: *Escherichia coli* BL21(DE3) chemical competent cells were heat-shock transformed with the plasmids pDULE_CNPheRS (1) and pCDFDuet1_*hs*Impβ^{Q220TAG}-sfGFP-His_6 or pCDFDuet1_*hs*Impβ^{Y255TAG}-sfGFP-His_6 and grown overnight in 100 mL of 2YT media with Spectinomycin (25 µg/mL) and Tetracyclin (12.5 µg/mL) with shaking at 220 rpm at 37°C. Next morning, 1 L 2YT media with Spectinomycin (25 µg/mL) and Tetracyclin (12.5 µg/mL) were inoculated at OD_{600} ~0.1 and grown till OD_{600} reached 0.2 – 0.3, when the unnatural amino acid AzF (1 mM, final) was added and the protein expression was induced by adding IPTG (500 µM, final) and let grow for another 5 h. The cells were harvested by centrifugation at 4,800 rotations per minute (rpm), snap frozen in liquid Nitrogen and stored at -80°C. The purification from the cell pellets is essentially the same as described above for *hs*Impβ-sfGFP.

Protein labeling: The purified *hs*Impβ-sfGFP Q220AzF was incubated on rocker at 4°C for 2 h with 200 µL bed volume of HisPur Ni-NTA beads (Thermo Fischer). The beads were washed twice with 1×PBS, pH 7.5 and 5 µL of freshly prepared 10 mg/mL of DBCO-Fl-545 was added. The mixture was incubated for another 2 h on rocker at 4°C, covered in aluminum foil. The beads were extensively washed with 1×PBS, pH 7.5 and finally eluted with 1×PBS,

pH 7.5 supplemented with 200 mM Imidazole. The labeled protein was directly loaded onto a Native-PAGE gel and scanned on Typhoon 9400 Variable Mode Imager. The region of the scanned image showing both sfGFP and Fl-545 emission was used as background to 'cut' the corresponding region from the Native-PAGE gel. The gel pieces were transferred to a D-Tube Dialyzer Midi (MerckMillipore) tube followed by electroelution in 25 mM Tris-Cl, pH 8.0, 100 mM NaCl and 1 mM ethylenediaminetetraacetic acid, on a horizontal gel electrophoresis system. The electroeluted protein was concentrated on a Vivaspin 500 centrifugal concentrator, glycerol (5% final) added, aliquoted in 10 µL volumes, snap frozen in liquid nitrogen and stored at -80°C.

Western blotting: The protein samples (10 or 20 µL) were run on a 8% Tris-Cl-SDS polyacrylamide gel electrophoresis (PAGE) gel, followed by transfer on Immobilon-P PVDF membrane for 50 min at 50 V. The membrane was blocked with 3% Bovine serum albumin prepared in 1 ×PBS, pH 7.5, for 30 min on rocker at 4°C followed by addition of mouse monoclonal anti-His antibody (1:10,000 dilution) in the above buffer, and incubating for additional 1 h. The membrane was washed three times with 30 mL of 1 ×PBS, pH 7.5, 0.02% Tween-20 for 10 minutes each and transferred in 5% skimmed milk in 1 ×PBS, pH 7.5. The HRP-conjugated anti-Mouse IgG (1:5,000 dilution) was added and incubated for 1 h at 4°C. The membrane was washed two times with 30 mL of 1 ×PBS, pH 7.5, 0.02% Tween-20 for 10 minutes each and once with 1 ×PBS, pH 7.5, 0.05% Tween-20 for 10 minutes. The ECL Prime solution was prepared as per manufacturer's protocol and spread on the membrane, and developed on a chemiluminescence Hyperfilm.

In-gel fluorescence: The Typhoon 9400 Variable Mode Imager (GE Lifesciences) was used for all the in-gel fluorescence scans. The settings for detecting sfGFP (excitation with 488 nm

blue laser, emission filter 520 nm, band pass 40 nm) and Fl-545 (excitation with 532 nm green laser, emission filter 580 nm, band pass 30 nm) was used. Additionally, different PMT gains (200 – 400 V) were used in conjugation with 100 or 200 µm resolution. The scanned images were processed with FluorSep 2.2 and/ or ImageQuant 5.2 (Molecular Dynamics) for visualization and preparing the 'merge' image (Figures 4, S5 and S7).

Nuclear import in permeabilized cells: For import of recombinant Impβ, 80.000 HeLa P4 cells (2) were grown on poly-L-lysine-coated cover slips, washed with cold transport buffer (TB, 20 mM HEPES pH 7.3, 110 mM KOAc, 2 mM $Mg(OAc)_2$, 1 mM EGTA, 1 µg/mL aprotinin, 1 µg/mL leupeptin, 1 µg/mL pepstatin, 2 mM DTT), and permeabilized on ice with 0.007% digitonin in TB. After three washing steps with TB, cells were incubated with Impβ-GFP proteins (diluted 1:20 from stock) at room temperature for 30 min in the presence of an energy-regenerating system (1 mM ATP, 5 mM creatine phosphate, 20 U/mL creatine phosphokinase) and 1 mg/mL BSA. After import, the cells were washed with TB and nuclei were stained with 2 µg/mL Hoechst 33258 (Sigma) in PBS for 2 min. The cover slips were dried and mounted with Dako Fluorescent Mounting Medium. Images were acquired with an LSM 510 META Laser Scanning Microscope (Carl Zeiss) and processed using the LSM image browser and Fiji.

Fluorescence Lifetime Measurements: Fluorescence lifetime measurements were performed on a MicroTime 200 confocal microscope system (PicoQuant, Berlin, Germany). The system is based on an inverse epi-fluorescence microscope (IX-71, Olympus Europa) with a water immersion objective (UPLSAPO 60 x W, 1.2 N.A., Olympus Hamburg, Germany). For fluorescence excitation and lifetime measurements, we used pulsed diode lasers (LDH-P-C-470, 470 nm, PicoQuant) with linear polarization, pulse duration of 50 psec (FWHM), 40

MHz repetition rate. Fluorescence excitation and detection is done through the same objective (epi-fluorescence configuration). Collected fluorescence light is passed through a dichroic mirror (490 dcxr, Chroma Technology, Rockingham, VT, USA), and then focused by a tube lens through a 150 µm diameter confocal pinhole. After the pinhole, the light is re-collimated, split by a 50/50 beam splitter, and focused onto two single photon avalanche diodes (tau-SPAD, PicoQuant, Berlin, Germany). Emission band-pass filters (HC520/35, Semrock, USA) are positioned in front of each detector to discriminate fluorescence against scattered light. Time-correlated single-photon counting electronics (HydraHarp 400, PicoQuant GmbH) record the detected photons of all detectors independently with an absolute temporal resolution of 32 psec on a common time frame. Data for all measurements were acquired for 15 min to achieve sufficiently good photon statistics.

The routines for fluorescence lifetime calculation and analysis were implemented in MATLAB (MathWorks, Inc.). A simple biexponential model was employed for fitting only the tail (> 1 ns after laser pulse) of the fluorescence decay curve. This analysis gives all information required for calculating FRET efficiencies by means of fluorescence life time change. The tail-fitting approach avoids all the complications associated with a full deconvolution of the fluorescence decay curve with an a priori measured instrumental response function, without reducing in any way the desired information about FRET efficiencies. FRET efficiencies were calculated from the difference between the mean lifetime value of the FRET sample and that of the donor-only control in the same buffer.

MD Simulations: All bonds were constrained using the LINCS algorithm (3). An integration time step of 2 fs was used. Lennard-Jones interactions were calculated with a cut-off of 10 Å. Electrostatic interactions were calculated explicitly at a distance smaller than 10 Å; long-range electrostatic interactions were calculated by particle-mesh Ewald summation with a grid spacing of 0.12 nm and fourth order B-spline interpolation. The temperature was kept at T =

300 K, using Berendsen coupling with a coupling time of τ_T = 0.1 ps (4). Structures were recorded every 1 ps for subsequent analysis. Simulations in water and in methanol were performed in the NPT ensemble. The pressure was coupled to a Berendsen barostat with τ_p = 1.0 ps and an isotropic compressibility of 4.5×10^{-5} bar^{-1} in the x, y, and z directions (4).

All systems were energy minimized, followed by relaxation for 500 ps at 300 K, with positional restraints on the protein heavy atoms by using a force constant of k = 1000 kJ mol^{-1} nm^{-2}. All simulations were performed using periodic boundary conditions.

Radii of gyration were calculated with the GROMACS tool *g_gyrate*. The statistical uncertainty of the averaged radii of gyration was estimated as follows:

For each of the *i* trajectories, the average radius of gyration, R^i_g and its standard deviation s_i were calculated. From these values, the standard errors of the mean (σ_i) were calculated as

$$\sigma_i = \frac{s_i}{\sqrt{t/\tau_i}},$$

where t_i is the length of the simulation and τ_i the autocorrelation time of the fluctuations of the radius of gyration. From the individual values of σ_i, an average error was calculated as

$$\sigma_A = \sqrt{\frac{1}{n}\sum_{i=1}^{n}\sigma_i^2},$$

where *n* is the number of individual trajectories. σ_A describes the error due to the fluctuations of R_g within each trajectory.

As a second source of statistical uncertainty, the error corresponding to the standard deviation *s* of the R^i_g values was calculated as

$$\sigma_B = \frac{s}{\sqrt{n}}.$$

For a conservative estimate of the overall statistical uncertainty we therefore assume

$$\sigma_A = \sqrt{\frac{1}{n}\sum_{i=1}^{n}\sigma_i^2} \quad .$$

Running averages were calculated with a Gaussian kernel of 1 ns width.

Supplementary Figure 1: Importin-β in aqueous solution.

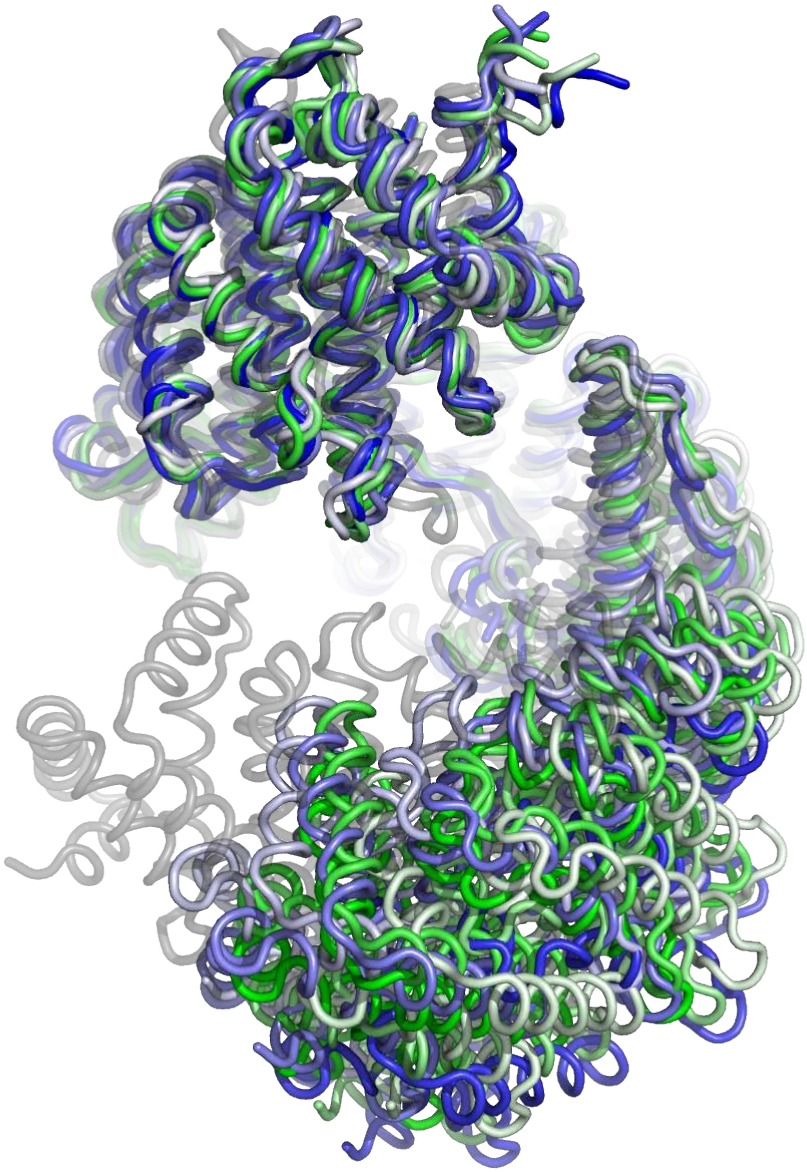

The most representative structures from a cluster analysis of Importin-β:sIBB (from the most populated cluster in green to the least populated one in blue) are aligned to the crystal structure (in grey) on the C-terminal arch.

Supplementary Figure 2: MD simulations in water.

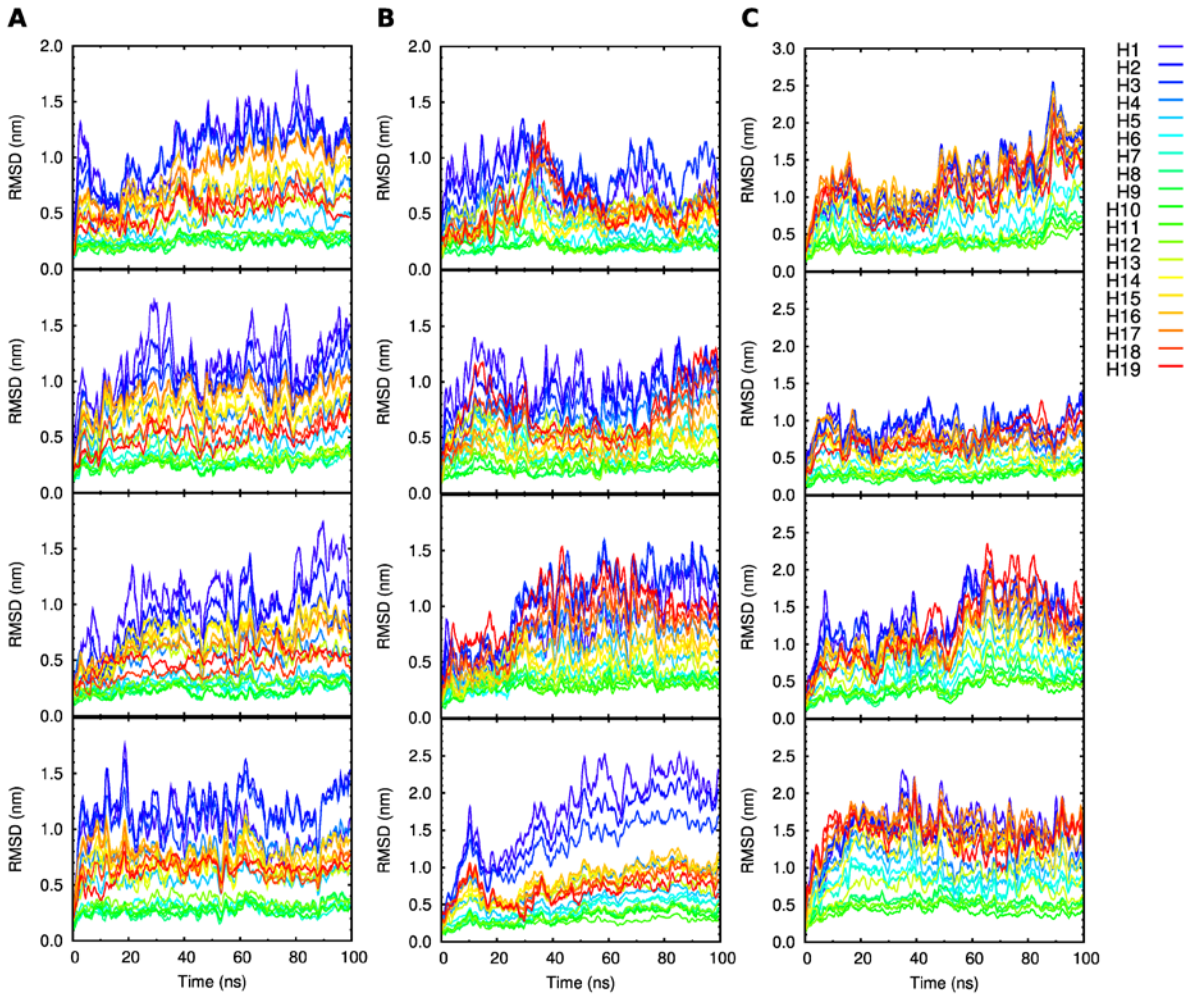

Change in root-mean-square deviation (RMSD) by HEAT repeats during simulation in water. (A) Importin-β:sIBB complex (B) Importin-β:αIBBcomplex (C) Free Importin-β (after removal of the sIBB domain). Four independent simulations each are shown. The structures were first aligned to the closed crystal structure using all backbone atoms, and, subsequently, the RMSD was calculated for each HEAT repeat separately.

Supplementary Figure 3: Simulated SAXS profile of free Importin-β in water.

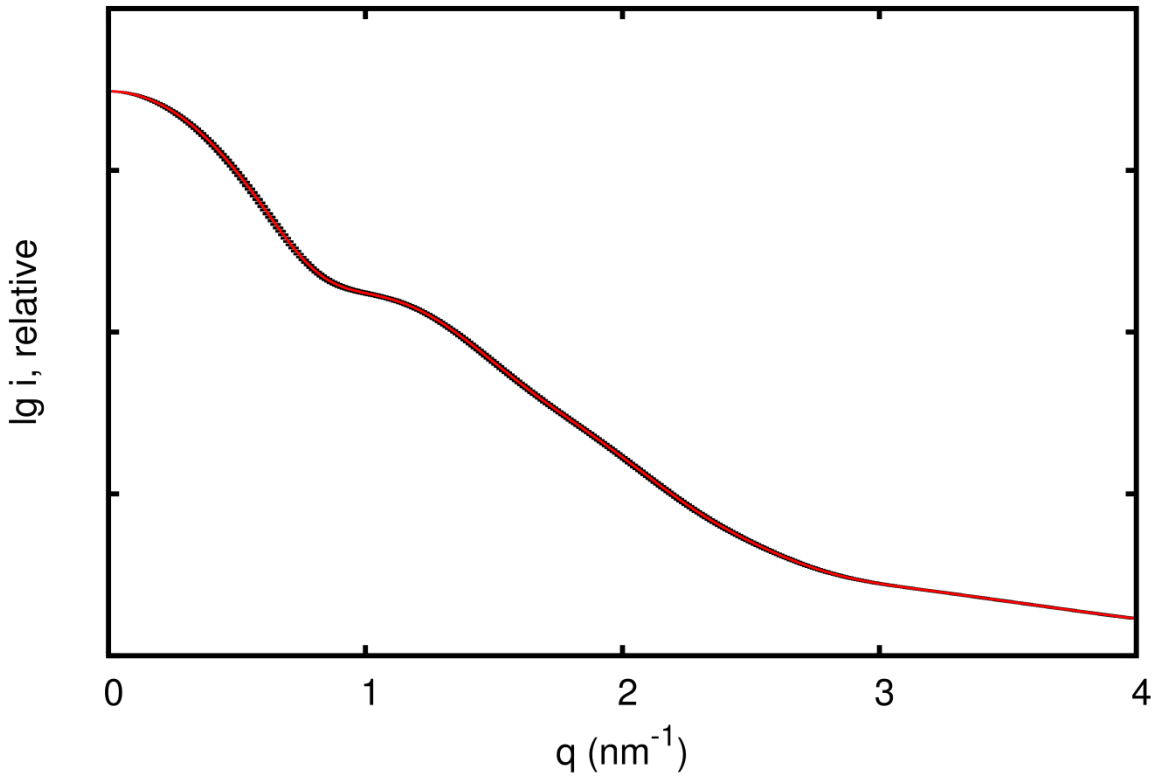

Scattering profiles were calculated on a total of 200 snapshots from the last 50 ns of the four independent trajectories and subsequently averaged. The errors were estimated by bootstrapping.

Supplementary Figure 4: MD simulations in methanol.

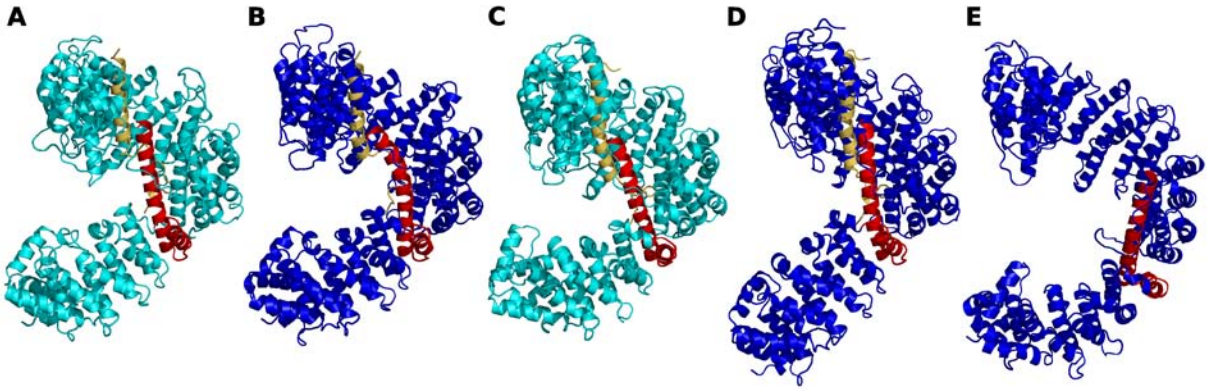

Starting conformations. (A, B) Importin-β:sIBB complex with undistorted (A) and distorted (B) HEAT repeats. (C, D) Importin-β:αIBB complex as half open (C) and completely open (D) structure. (E) Free Importin-β. H7 is shown in red, the IBB domains are shown in yellow.

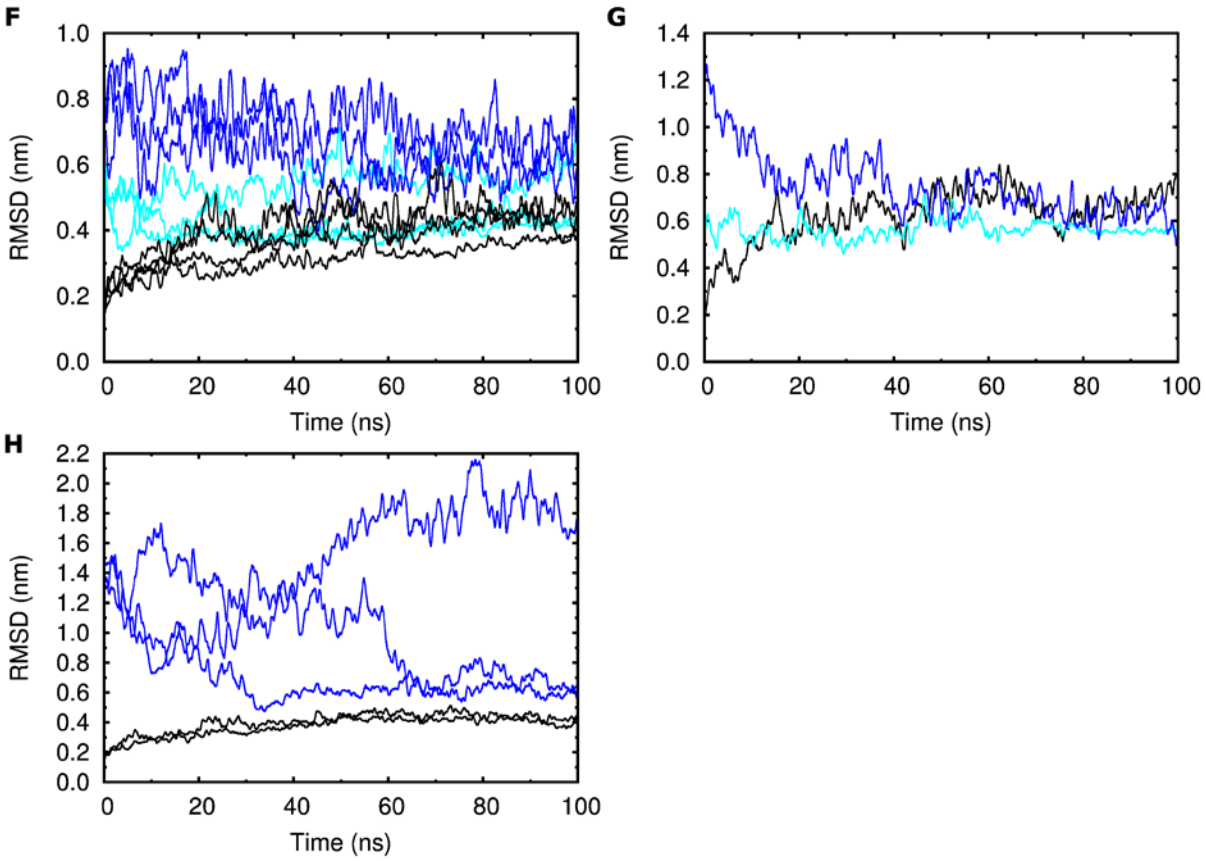

Changes in root-mean-square deviation (RMSD) during the simulations. RMSD with respect to the corresponding closed crystal structure for Importin-β:sIBB (F), Importin-β:αIBB (G), and free Importin-β (H). Simulations started from open (blue), undistorted half open (cyan) and closed (black) conformations.

Supplementary Figure 5: Spectral properties of *hs*Importin-β-sfGFP.

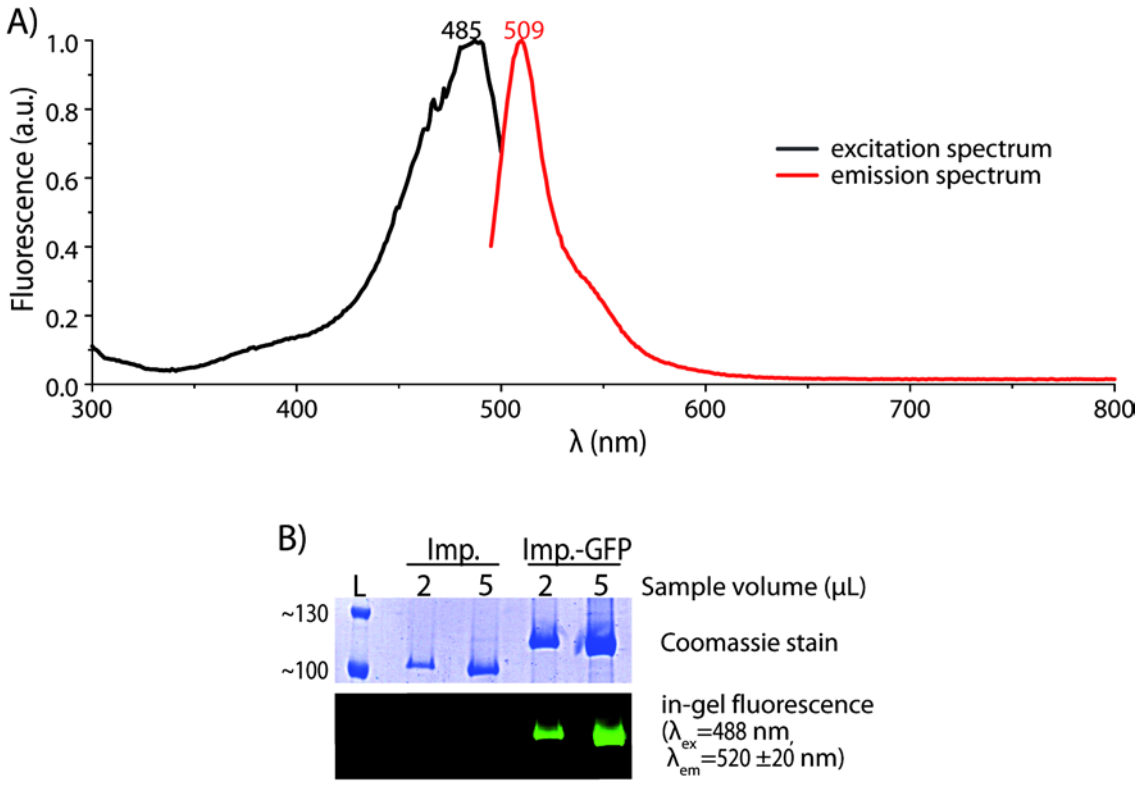

A) Excitation and emission spectra of *hs*Importin-β-GFP. B) In-gel fluorescence spectrum of *hs*Importin-β-sfGFP. L: Prestained Protein Ladder.

Supplementary Figure 6: Incorporation of AzF in hsImportin-β.

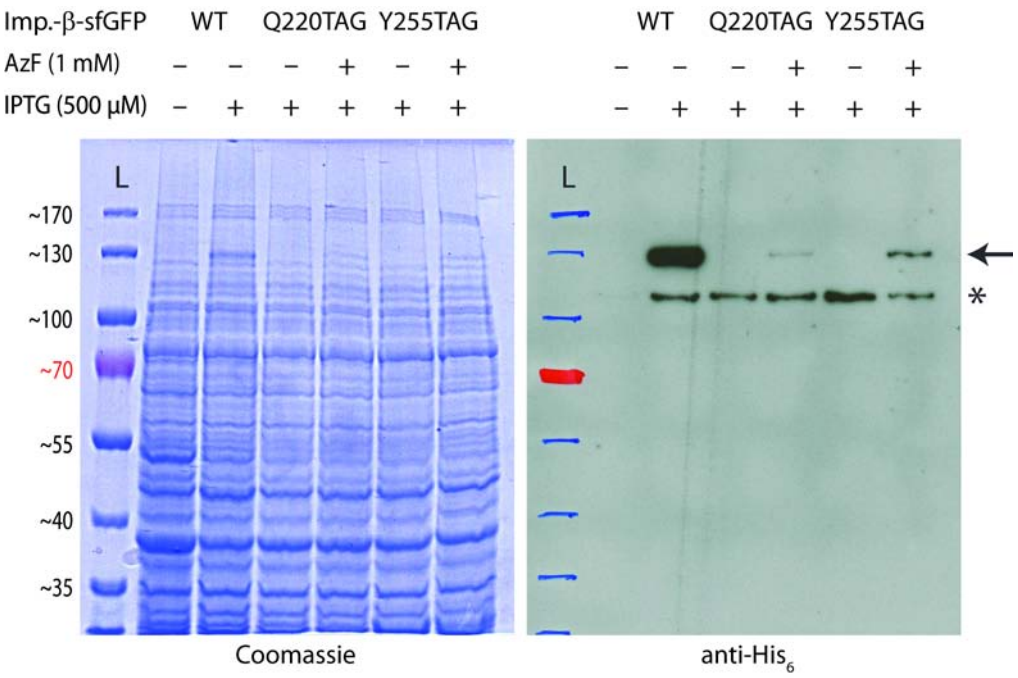

BL21 DE3 cells were transformed with plasmids encoding *hs*Importin-β with amber codons replacing codons Q220 or Y255 and pDULE CNPheRS. Cells were grown in the presence or absence of IPTG and AzF as indicated and analyzed by SDS-PAGE and Western blot. Arrow indicates the position of *hs*Importin-β, an unspecific anti-His_6 antibody cross-reactive band is indicated by an asterisk.

Supplementary Figure 7: Purification and labeling of *hs*Importin-β-sfGFP.

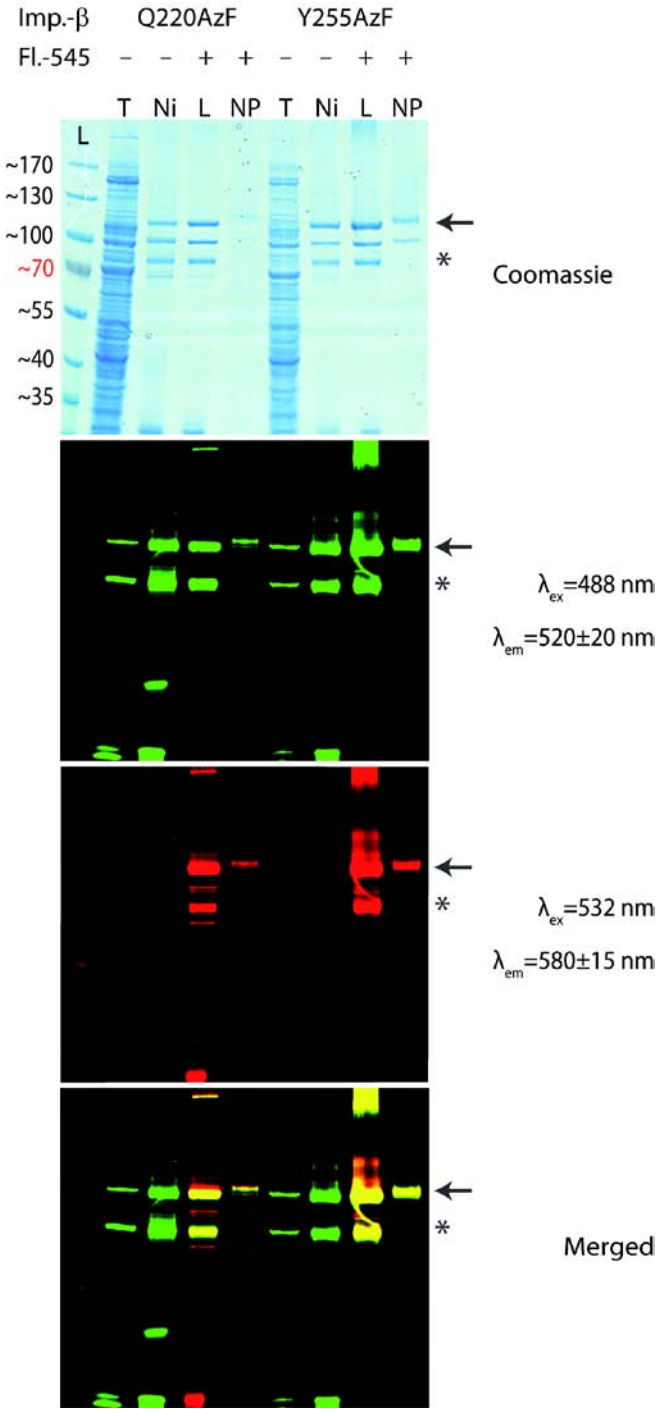

*hs*Importin-β-GFP proteins were extracted (T), purified by Ni^{2+}-affinity chromatography (Ni), labeled with Fl.-545-DBCO (L) and purified by native-PAGE (NP). Samples from all stages were analyzed by SDS-PAGE and in-gel fluorescence measured on a Typhoon phosphoimager. Arrow indicates the position of full-length *hs*Importin-β, a proteolytic fragment of *hs*Importin-β is indicated by an asterisk.

Supplementary Figure 8: Fluorescence emission spectra of *hs*Importin-β-sfGFP and *hs*Importin-β-GFP Q220AzF-Fl.-545.

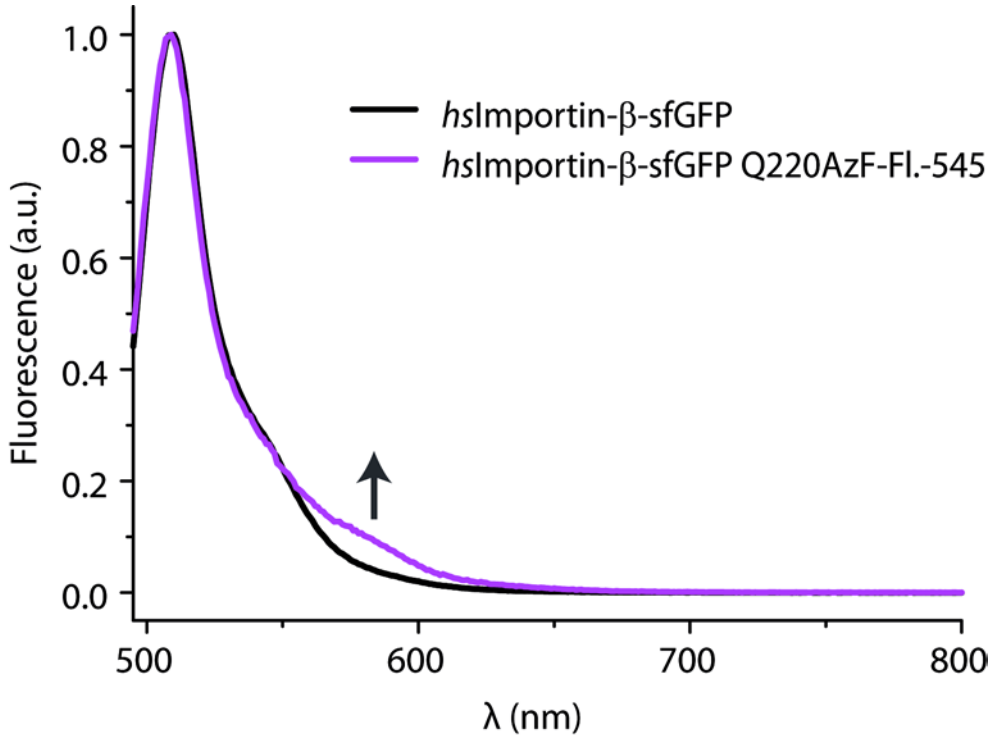

Fluorescence emission spectra of *hs*Importin-β-sfGFP and *hs*Importin-β-GFP Q220AzF-Fl.-545 were acquired using $\lambda_{ex.}$=470 nm. Coupling of the fluorophore leads to an increased emission at 575 nm.

Supplementary Figure 9: FRET in *hs*Importin-β-sfGFP Q220AzF-Fl.-545 is Proteinase K sensitive.

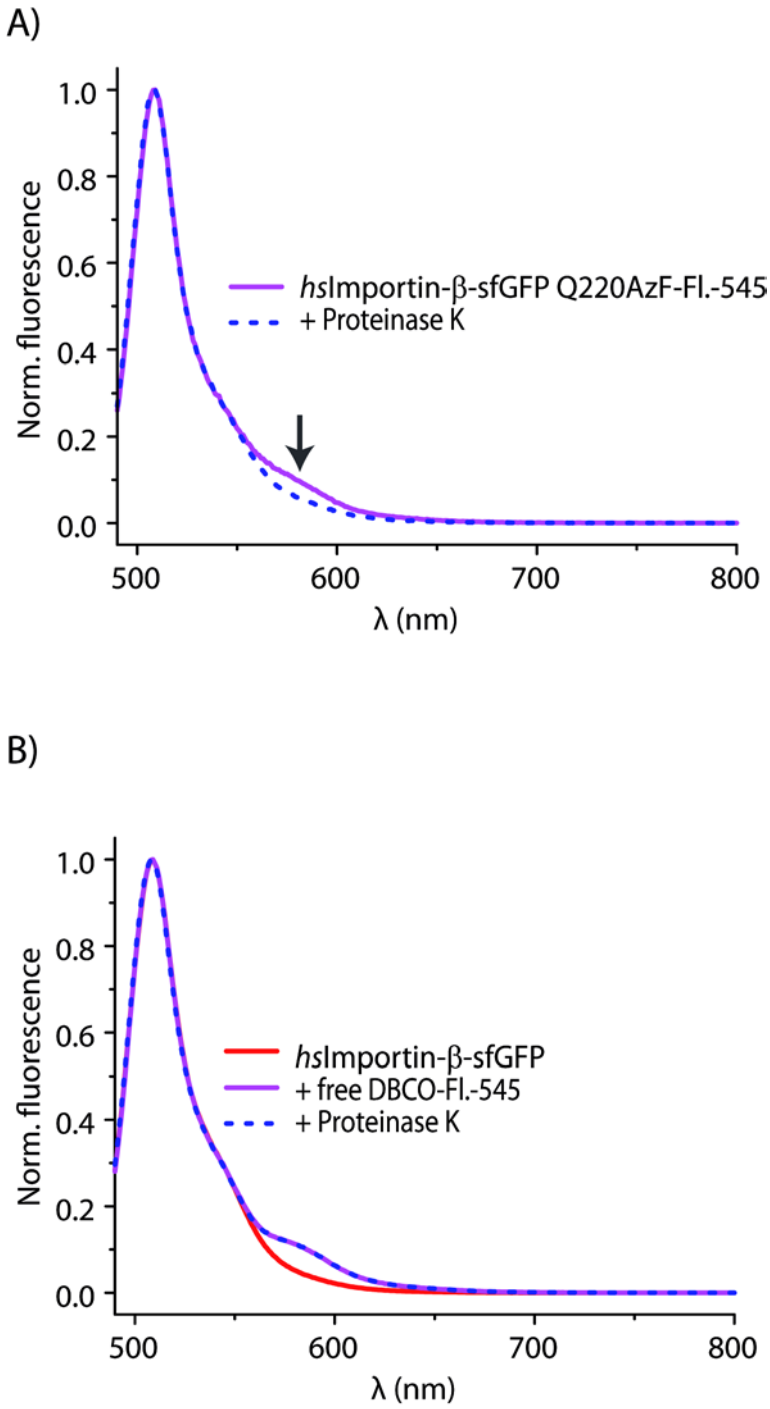

A) Fluorescence emission scans of *hs*Importin-β-sfGFP Q220AzF-Fl.-545 were taken before and after treatment with Proteinase K. B) Fluorescence emission scans of *hs*Importin-β-sfGFP were taken before and after the addition of free DBCO-Fl.-545 dye and after subsequent treatment with Proteinase K.

Supplementary Figure 10: Localization of *hs*Importin-β-sfGFP Q220AzF-Fl.-545 in permeabilized HeLa cells.

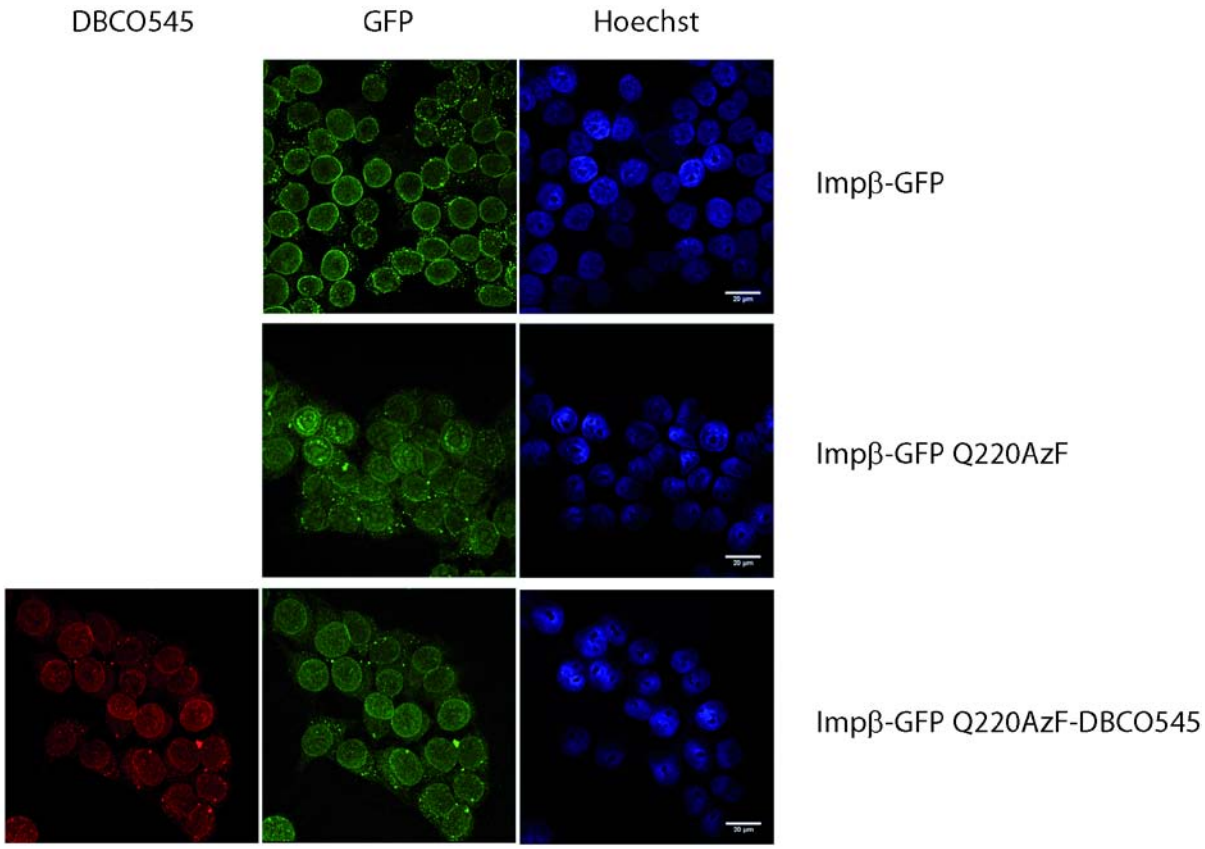

Permeabilized HeLa cells were incubated with indicated purified proteins, stained with Hoechst dye and imaged by fluorescence microscopy.

Supplementary Figure 11: Titration of methanol induces FRET in *hs*Importin-β-sfGFP Q220AzF-Fl.-545.

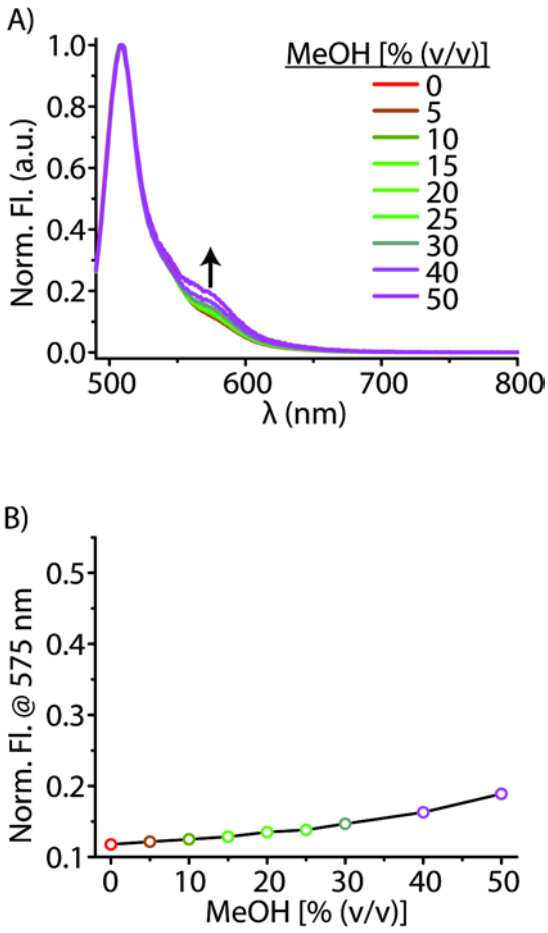

A-B) Increasing concentrations of methanol were added to *hs*Importin-β-sfGFP Q220AzF-Fl.-545. Between each addition fluorescence emission scans were acquired. Fluorescence was normalized for each spectrum setting the highest peak to 1.0.

Supplementary Figure 12: Addition of PEG induces increased FRET in *hs*Importin-β-sfGFP Q220AzF-Fl.-545.

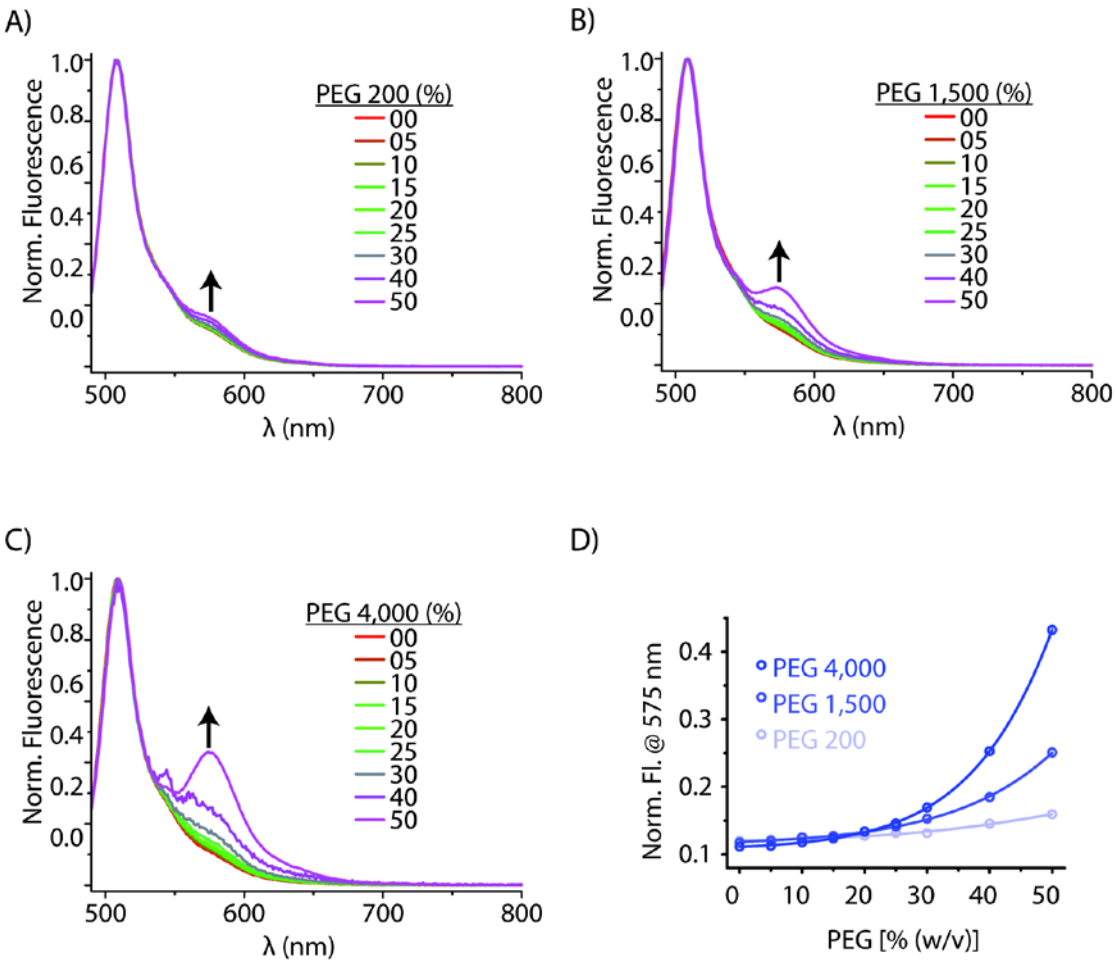

A-C) Increasing amounts of PEG of the indicated molecular weight were added to *hs*Importin-β-sfGFP Q220AzF-Fl.-545. Between each addition fluorescence emission scans were acquired. Fluorescence was normalized for each spectrum setting the highest peak to 1.0. D) Emission intensities at 575 nm of panels A-C were plotted against PEG concentration.

Supplementary Figure 13: Increasing PEG concentrations do not affect individual fluorophore properties.

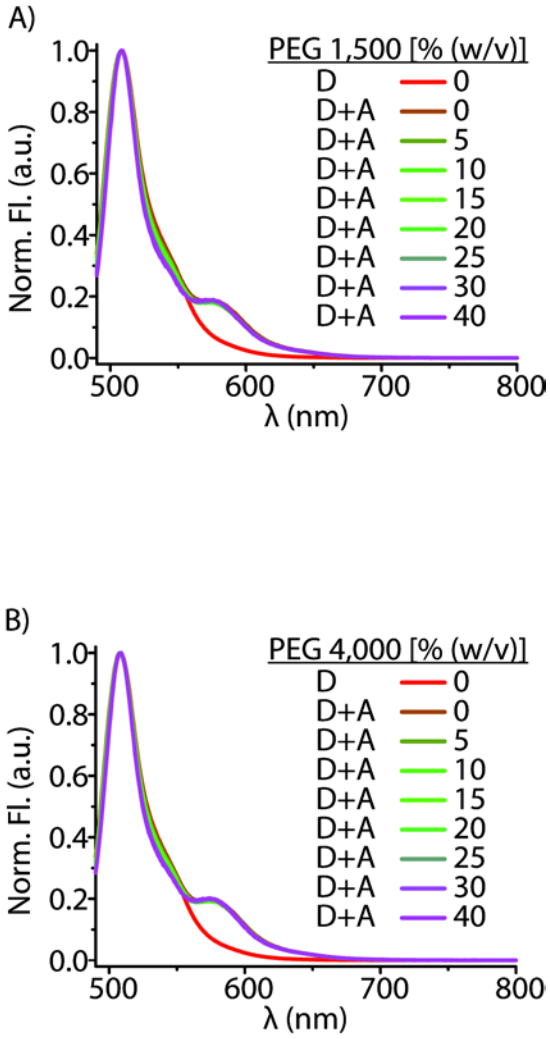

Increasing PEG concentrations do not affect the individual fluorescence properties of donor (D, *hs*Importin-β-sfGFP) and acceptor (A, DBCO-Fl.-545) dyes. A-B) *hs*Importin-β-sfGFP and DBCO-Fl.-545 were mixed in buffer and increasing concentrations of PEG of the indicated molecular weight were added stepwise. Between each addition fluorescence emission spectra were acquired ($\lambda_{ex.}$=470 nm).

Supplementary Figure 14: Titration of Ficoll-70 does not induce significantly increased FRET in *hs*Importin-β-sfGFP Q220AzF-Fl.-545.

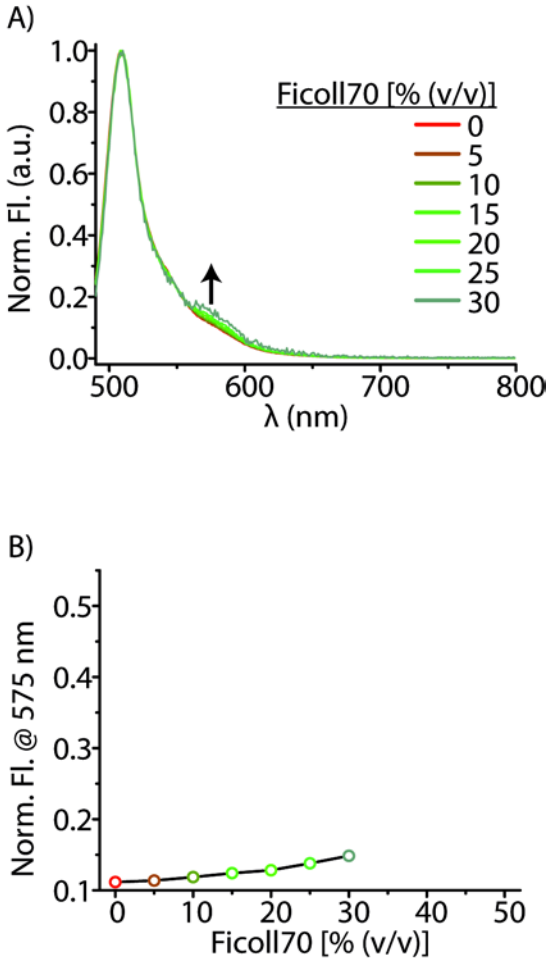

A) Increasing amounts of Ficoll-70 was added to *hs*Importin-β-sfGFP Q220AzF-Fl.-545. Between each addition fluorescence emission scans were acquired. Fluorescence was normalized for each spectrum setting the highest peak to 1.0. B) Emission intensities at 575 nm of panel A was plotted against Ficoll-70 concentration. For technical reasons a concentration above 30% could not be reached.

Supplementary Figure 15: Reversibility of PEG induced FRET increase in *hs*Importin-β-sfGFP Q220AzF-Fl.-545.

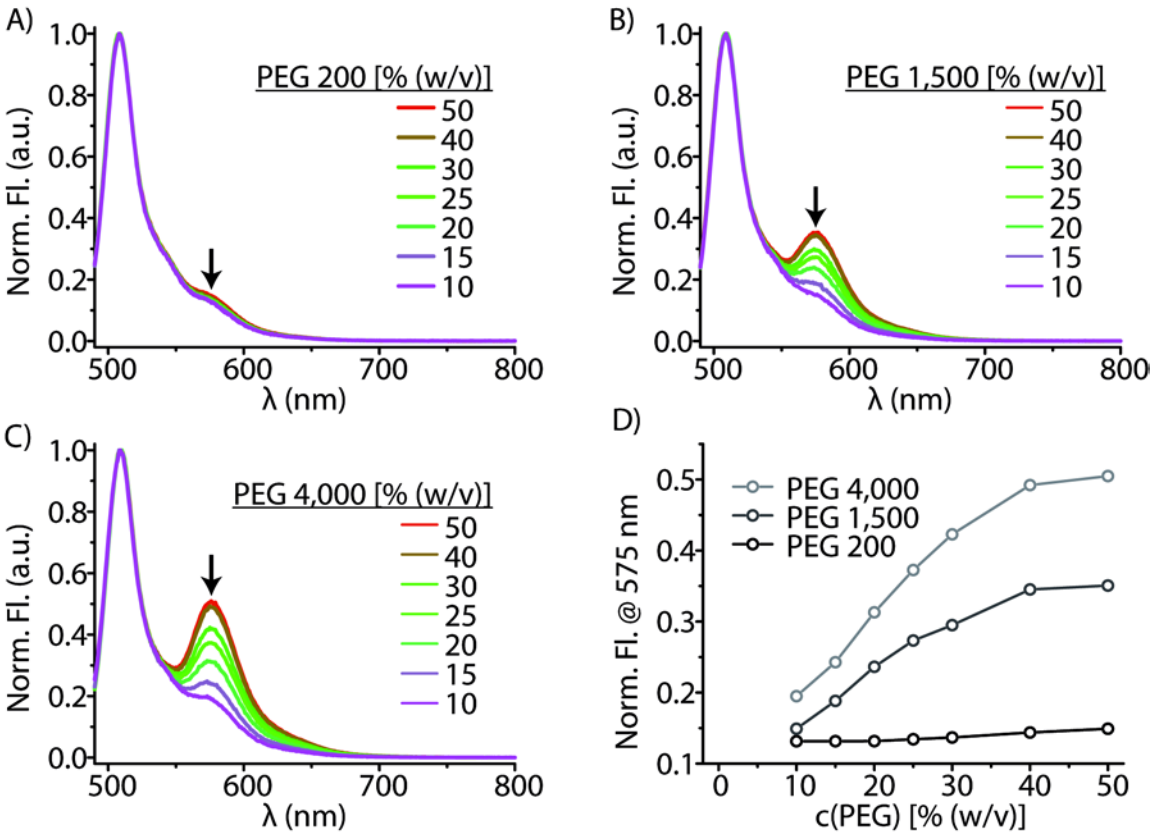

A-C) Starting from a *hs*Importin-β-sfGFP Q220AzF-Fl.-545 solution containing a concentration of 50% PEG of the indicated molecular weight buffer is added stepwise. Between each addition fluorescence emission scans were acquired. Fluorescence was normalized for each spectrum setting the highest peak to 1.0. D) Emission intensities at 575 nm of panels A-C were plotted against PEG concentration.

Supplementary Figure 16: Donor fluorescence lifetime measurements.

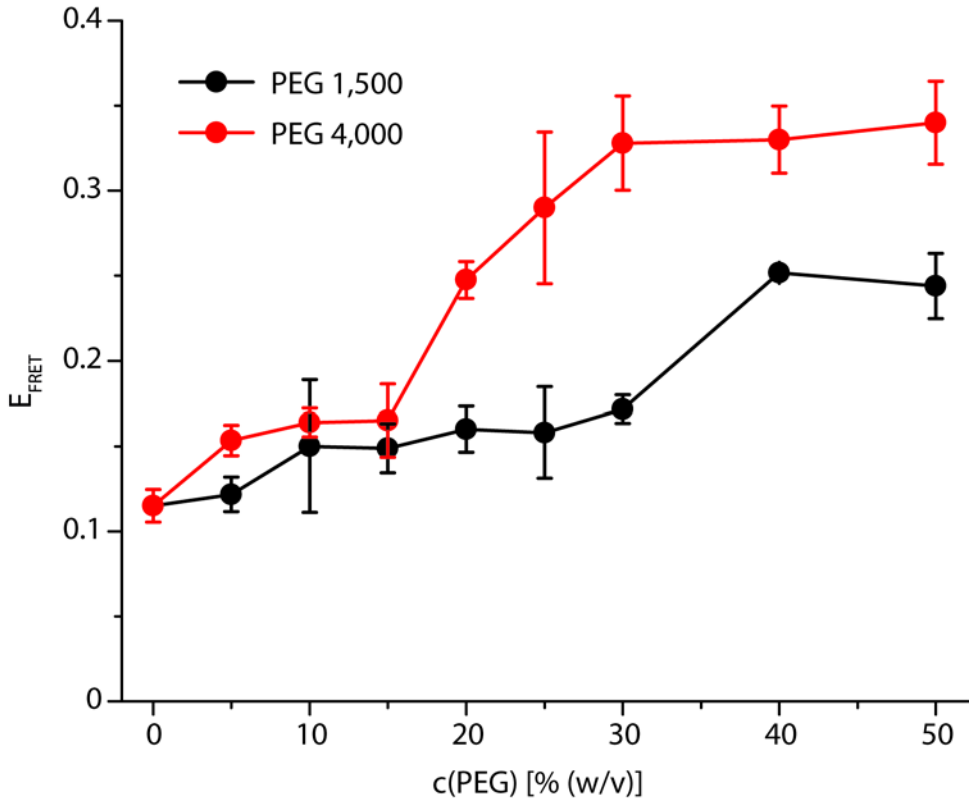

Addition of PEG 1,500 or PEG 4,000 increases relative FRET efficiency in *hs*Impβ-sfGFP Q220AzF-Fl.-545 determined by donor fluorescence lifetime measurements. Error bars represent standard error of the mean.

Supplementary Table S1

Importin-β in complex with	Simulations in water	Simulations in methanol
sIBB	4 x 100 ns (PDBid 2P8Q)	4 x 100 ns (PDBid 2P8Q) 3 x 100 ns (snapshot from simulations in water, Rg=3.4 nm, undistorted) 3 x 100 ns (snapshot from simulations in water, Rg=3.5 nm, distorted)
αIBB	4 x 100 ns (PDBid 2QGK)	1 x 100 ns (PDBid 2QGK) 1 x 100 ns (snapshot from simulations in water, Rg=3.4 nm) 1 x 100 ns (snapshot from simulations in water, Rg=3.7 nm)
---	3 x 100 ns (PDBid 2P8Q, after removal of sIBB) 1 x 100 ns (PDBid 2QGK, after removal of αIBB)	2 x 100 ns (PDBid 2P8Q, after removal of sIBB) 3 x 100 ns (snapshot from simulations in water, Rg=3.9 nm)

Table S1: Summary of simulations with their corresponding initial conformations (in parentheses).

Supplementary Table S2

PDBid	Importin-β in complex with	Crystallization condition Mother liquor	Cryo condition in addition to mother liquor	Confor-mation
1QGK (5)	αIBB	18-22% PEG 8000, 50 mM potassium acetate (pH 5.8), 10 mM β-mercaptoethanol	prolonged dehydration (1-7 days) 25% PEG 400	closed
1QGR (5)	αIBB	16-20% PEG 8000, 50 mM potassium phosphate (pH 3.9), 10 mM β-mercaptoethanol, 5 mM NaI	prolonged dehydration 25% PEG 400	closed

1UKL (6)	SREBP-2	5-6% PEG 8000, 10% glycerol, 50 mM MES buffer (pH 6.6), 30 mM $SrCl_2$	25% glycerol	open
2BKU (7)	RanGTP	14-16% PEG 3350, 100 mM MES buffer (pH 6.2), 1-2 mM MnCl	25% (w/v) glycerol	open
2BPT (8)	Nup1p	13% (w/v) PEG 8000, 5 mM Tris (pH 7.4), 50 mM sodium cacodylate (pH 6.5), 90 mM $(NH_4)_2SO_4$	10% (w/v) glycerol	closed
2P8Q (9)	sIBB	20% PEG 8000, 50 mM NaCl (pH 6.0)	prolonged dehydration 38% PEG 8000	closed
2Q5D (9)	sIBB	20% PEG 8000, 50 mM NaCl (pH 6.0)	prolonged dehydration 38% PEG 8000	closed/ open
3ND2 (10)		20% PEG 4000, 12% MPD, 0.1 M MES (pH 6.5), 20 mM $MgCl_2$, 125 mM NaCl		closed
2QNA (11)	sIBB	0.92 M $(NH_4)_2SO_4$, 2.5% ethanol	quick soak (seconds) 20% glycerol to mother liquor	open

Table S2: Comparison of crystallization conditions and Importin-β conformation.

Plasmid Sequence of pCDFDuet1_*hs*Impβ-sfGFP-His$_6$, pCDFDuet1_*hs*Impβ^{Q220TAG}-sfGFP-His$_6$ and pCDFDuet1_*hs*Impβ^{Y255TAG}-sfGFP-His$_6$: The ORF (nucleotide 71 – 3,451) is shown in lowercase and the TAG mutation sites for amino acid Q220 and Y255 is highlighted in yellow and green, respectively:

```
   1 GGGGAATTGTGAGCGGATAACAATTCCCCTGTAGAAATAATTTTGTTTAACTTTAATAAG 60
  61 GAGATATAccatggagctgatcaccattctcgagaagaccgtgtctcccgatcggctgga 120
 121 gctggaagcggcgcagaagttcctggagcgtgcggccgtggagaacctgcccactttcct 180
 181 tgtggaactgtccagagtgctggcaaatccaggaaacagtcaggttgccagagttgcagc 240
 241 tggtctacaaatcaagaactctttgacatctaaagatccagatatcaaggcacaatatca 300
 301 gcagaggtggcttgctattgatgctaatgctcgacgagaagtcaagaactatgttttgca 360
 361 gacattgggtacagaaacttaccggcctagttctgcctcacagtgtgtggctggtattgc 420
 421 ttgtgcagagatcccagtaaaccagtggccagaactcattcctcagctggtggccaatgt 480
 481 cacaaaccccaacagcacagagcacatgaaggagtcgacattggaagccatcggttatat 540
 541 ttgccaagatatagacccagagcagctacaagataaatccaatgagattctgactgccat 600
 601 aatccaggggatgaggaaagaagagcctagtaataatgtgaagctagctgctacgaatgc 660
 661 actcctgaactcattggagttcaccaaagcaaactttgataaagagtctgaaaggcactt 720
 721 tattatgcaggtggtctgtgaagccacacagtgtccagatacgagggtacgagtggctgc 780
 781 tttacagaatctggtgaagataatgtccttatattatcagtacatggagacatatatggg 840
 841 tcctgctctttttgcaatcacaatcgaagcaatgaaaagtgacattgatgaggtggcttt 900
 901 acaagggatagaattctggtccaatgtctgtgatgaggaaatggatttggccattgaagc 960
 961 ttcagaggcagcagaacaaggacggccccctgagcacaccagcaagttttatgcgaaggg 1020
1021 agcactacagtatctggttccaatcctcacacagacactaactaaacaggacgaaaatga 1080
1081 tgatgacgatgactggaacccctgcaaagcagcaggggtgtgcctcatgcttctggccac 1140
1141 ctgctgtgaagatgacattgtcccacatgtcctccccttcattaaagaacacatcaagaa 1200
1201 cccagattggcggtaccgggatgcagcagtgatggcttttggttgtatcttggaaggacc 1260
1261 agagcccagtcagctcaaaccactagttatacaggctatgcccaccctaatagaattaat 1320
1321 gaaagaccccagtgtagttgttcgagatacagctgcatggactgtaggcagaatttgtga 1380
1381 gctgcttcctgaagctgccatcaatgatgtctacttggctcccctgctacagtgtctgat 1440
1441 tgagggtctcagtgctgaacccagagtggcttcaaatgtgtgctgggctttctccagtct 1500
1501 ggctgaagctgcttatgaagctgcagacgttgctgatgatcaggaagaaccagctactta 1560
1561 ctgcttatcttcttcatttgaactcatagttcagaagctcctagagactacagacagacc 1620
1621 tgatggacaccagaacaacctgaggagttctgcatatgaatctctgatggaaattgtgaa 1680
1681 aaacagtgccaaggattgttatcctgctgtccagaaaacgactttggtcatcatggaacg 1740
1741 actgcaacaggttcttcagatggagtcacatatccagagcacatccgatagaatccagtt 1800
1801 caatgaccttcagtctttactctgtgcaactcttcagaatgttcttcggaaagtgcaaca 1860
1861 tcaagatgctttgcagatctctgatgtggttatggcctccctgttaaggatgttccaaag 1920
1921 cacagctgggtctgggggagtacaagaggatgccctgatggcagttagcacactggtgga 1980
1981 agtgttgggtggtgaattcctcaagtacatggaggcctttaaacccttcctgggcattgg 2040
2041 attaaaaaattatgctgaataccaggtttgtttggcagctgtgggcttagtgggagactt 2100
2101 gtgccgtgccctgcaatccaacatcatacctttctgtgacgaggtgatgcagctgcttct 2160
2161 ggaaaatttggggaatgagaacgtccacaggtctgtgaagccgcagattctgtcagtgtt 2220
2221 tggtgatattgcccttgctattggaggagagtttaaaaaatacttagaggttgtattgaa 2280
2281 tactcttcagcaggcctcccaagcccaggtggacaagtcagactatgacatggtggatta 2340
2341 tctgaatgagctaagggaaagctgcttggaagcctatactggaatcgtccagggattaaa 2400
2401 gggggatcaggagaacgtacacccggatgtgatgctggtacaacccagagtagaatttat 2460
2461 tctgtctttcattgaccacattgctggagatgaggatcacacagatggagtagtagcttg 2520
2521 tgctgctggactaataggggacttatgtacagcatttgggaaggatgtactgaaattagt 2580
2581 agaagctaggccaatgatccatgaattgttaactgaagggcggagatcgaagactaacaa 2640
2641 agcaaaaacccttgctacatgggcaacaaaagaactgaggaaactgaagaaccaagctgg 2700
2701 atctCAATTGgttagcaaaggtgaagaactgtttaccggcgttgtgccgattctggtgga 2760
2761 actggatggtgatgtgaatggccataaatttagcgttcgtggcgaaggcgaaggtgatgc 2820
2821 gaccaacggtaaactgaccctgaaatttatttgcaccaccggtaaactgccggttccgtg 2880
2881 gccgaccctggtgaccaccctgacctatggcgttcagtgctttagccgctatccggatca 2940
2941 tatgaaacgccatgatttctttaaaagcgcgatgccggaaggctatgtgcaggaacgtac 3000
3001 cattagcttcaaagatgatggcacctataaaacccgtgcggaagttaaatttgaaggcga 3060
```

3061 taccctggtgaaccgcattgaactgaaaggtattgattttaaagaagatggcaacattct 3120
3121 gggtcataaactggaatataatttcaacagccataatgtgtatattaccgccgataaaca 3180
3181 gaaaaatggcatcaaagcgaactttaaaatccgtcacaacgtggaagatggtagcgtgca 3240
3241 gctggcggatcattatcagcagaataccccgattggtgatggcccggtgctgctgccgga 3300
3301 taatcattatctgagcacccagagcgttctgagcaaagatccgaatgaaaaacgtgatca 3360
3361 tatggtgctgctggaatttgttaccgccgcgggcattacccacggtatggatgaactgta 3420
3421 taaaggcagccaccatcatcatcaccattaaGACGTCGGTACCCTCGAGTCTGGTAAAGA 3480
3481 AACCGCTGCTGCGAAATTTGAACGCCAGCACATGGACTCGTCTACTAGCGCAGCTTAATT 3540
3541 AACCTAGGCTGCTGCCACCGCTGAGCAATAACTAGCATAACCCCTTGGGGCCTCTAAACG 3600
3601 GGTCTTGAGGGGTTTTTTGCTGAAACCTCAGGCATTTGAGAAGCACACGGTCACACTGCT 3660
3661 TCCGGTAGTCAATAAACCGGTAAACCAGCAATAGACATAAGCGGCTATTTAACGACCCTG 3720
3721 CCCTGAACCGACGACCGGGTCATCGTGGCCGGATCTTGCGGCCCCTCGGCTTGAACGAAT 3780
3781 TGTTAGACATTATTTGCCGACTACCTTGGTGATCTCGCCTTTCACGTAGTGGACAAATTC 3840
3841 TTCCAACTGATCTGCGCGCGAGGCCAAGCGATCTTCTTCTTGTCCAAGATAAGCCTGTCT 3900
3901 AGCTTCAAGTATGACGGGCTGATACTGGGCCGGCAGGCGCTCCATTGCCCAGTCGGCAGC 3960
3961 GACATCCTTCGGCGCGATTTTGCCGGTTACTGCGCTGTACCAAATGCGGGACAACGTAAG 4020
4021 CACTACATTTCGCTCATCGCCAGCCCAGTCGGGCGGCGAGTTCCATAGCGTTAAGGTTTC 4080
4081 ATTTAGCGCCTCAAATAGATCCTGTTCAGGAACCGGATCAAAGAGTTCCTCCGCCGCTGG 4140
4141 ACCTACCAAGGCAACGCTATGTTCTCTTGCTTTTGTCAGCAAGATAGCCAGATCAATGTC 4200
4201 GATCGTGGCTGGCTCGAAGATACCTGCAAGAATGTCATTGCGCTGCCATTCTCCAAATTG 4260
4261 CAGTTCGCGCTTAGCTGGATAACGCCACGGAATGATGTCGTCGTGCACAACAATGGTGAC 4320
4321 TTCTACAGCGCGGAGAATCTCGCTCTCTCCAGGGGAAGCCGAAGTTTCCAAAAGGTCGTT 4380
4381 GATCAAAGCTCGCCGCGTTGTTTCATCAAGCCTTACGGTCACCGTAACCAGCAAATCAAT 4440
4441 ATCACTGTGTGGCTTCAGGCCGCCATCCACTGCGGAGCCGTACAAATGTACGGCCAGCAA 4500
4501 CGTCGGTTCGAGATGGCGCTCGATGACGCCAACTACCTCTGATAGTTGAGTCGATACTTC 4560
4561 GGCGATCACCGCTTCCCTCATACTCTTCCTTTTTCAATATTATTGAAGCATTTATCAGGG 4620
4621 TTATTGTCTCATGAGCGGATACATATTTGAATGTATTTAGAAAAATAAACAAATAGCTAG 4680
4681 CTCACTCGGTCGCTACGCTCCGGGCGTGAGACTGCGGCGGGCGCTGCGGACACATACAAA 4740
4741 GTTACCCACAGATTCCGTGGATAAGCAGGGGACTAACATGTGAGGCAAAACAGCAGGGCC 4800
4801 GCGCCGGTGGCGTTTTTCCATAGGCTCCGCCCTCCTGCCAGAGTTCACATAAACAGACGC 4860
4861 TTTTCCGGTGCATCTGTGGGAGCCGTGAGGCTCAACCATGAATCTGACAGTACGGGCGAA 4920
4921 ACCCGACAGGACTTAAAGATCCCCACCGTTTCCGGCGGGTCGCTCCCTCTTGCGCTCTCC 4980
4981 TGTTCCGACCCTGCCGTTTACCGGATACCTGTTCCGCCTTTCTCCCTTACGGGAAGTGTG 5040
5041 GCGCTTTCTCATAGCTCACACACTGGTATCTCGGCTCGGTGTAGGTCGTTCGCTCCAAGC 5100
5101 TGGGCTGTAAGCAAGAACTCCCCGTTCAGCCCGACTGCTGCGCCTTATCCGGTAACTGTT 5160
5161 CACTTGAGTCCAACCCGGAAAAGCACGGTAAAACGCCACTGGCAGCAGCCATTGGTAACT 5220
5221 GGGAGTTCGCAGAGGATTTGTTTAGCTAAACACGCGGTTGCTCTTGAAGTGTGCGCCAAA 5280
5281 GTCCGGCTACACTGGAAGGACAGATTTGGTTGCTGTGCTCTGCGAAAGCCAGTTACCACG 5340
5341 GTTAAGCAGTTCCCCAACTGACTTAACCTTCGATCAAACCACCTCCCCAGGTGGTTTTTT 5400
5401 CGTTTACAGGGCAAAAGATTACGCGCAGAAAAAAAGGATCTCAAGAAGATCCTTTGATCT 5460
5461 TTTCTACTGAACCGCTCTAGATTTCAGTGCAATTTATCTCTTCAAATGTAGCACCTGAAG 5520
5521 TCAGCCCCATACGATATAAGTTGTAATTCTCATGTTAGTCATGCCCCGCGCCCACCGGAA 5580
5581 GGAGCTGACTGGGTTGAAGGCTCTCAAGGGCATCGGTCGAGATCCCGGTGCCTAATGAGT 5640
5641 GAGCTAACTTACATTAATTGCGTTGCGCTCACTGCCCGCTTTCCAGTCGGGAAACCTGTC 5700
5701 GTGCCAGCTGCATTAATGAATCGGCCAACGCGCGGGGAGAGGCGGTTTGCGTATTGGGCG 5760
5761 CCAGGGTGGTTTTTCTTTTCACCAGTGAGACGGGCAACAGCTGATTGCCCTTCACCGCCT 5820
5821 GGCCCTGAGAGAGTTGCAGCAAGCGGTCCACGCTGGTTTGCCCCAGCAGGCGAAAATCCT 5880
5881 GTTTGATGGTGGTTAACGGCGGGATATAACATGAGCTGTCTTCGGTATCGTCGTATCCCA 5940
5941 CTACCGAGATGTCCGCACCAACGCGCAGCCCGGACTCGGTAATGGCGCGCATTGCGCCCA 6000
6001 GCGCCATCTGATCGTTGGCAACCAGCATCGCAGTGGGAACGATGCCCTCATTCAGCATTT 6060
6061 GCATGGTTTGTTGAAAACCGGACATGGCACTCCAGTCGCCTTCCCGTTCCGCTATCGGCT 6120
6121 GAATTTGATTGCGAGTGAGATATTTATGCCAGCCAGCCAGACGCAGACGCGCCGAGACAG 6180
6181 AACTTAATGGGCCCGCTAACAGCGCGATTTGCTGGTGACCCAATGCGACCAGATGCTCCA 6240
6241 CGCCCAGTCGCGTACCGTCTTCATGGGAGAAAATAATACTGTTGATGGGTGTCTGGTCAG 6300
6301 AGACATCAAGAAATAACGCCGGAACATTAGTGCAGGCAGCTTCCACAGCAATGGCATCCT 6360
6361 GGTCATCCAGCGGATAGTTAATGATCAGCCCACTGACGCGTTGCGCGAGAAGATTGTGCA 6420
6421 CCGCCGCTTTACAGGCTTCGACGCCGCTTCGTTCTACCATCGACACCACCACGCTGGCAC 6480
6481 CCAGTTGATCGGCGCGAGATTTAATCGCCGCGACAATTTGCGACGGCGCGTGCAGGGCCA 6540
6541 GACTGGAGGTGGCAACGCCAATCAGCAACGACTGTTTGCCCGCCAGTTGTTGTGCCACGC 6600
6601 GGTTGGGAATGTAATTCAGCTCCGCCATCGCCGCTTCCACTTTTTCCCGCGTTTTCGCAG 6660
6661 AAACGTGGCTGGCCTGGTTCACCACGCGGGAAACGGTCTGATAAGAGACACCGGCATACT 6720
6721 CTGCGACATCGTATAACGTTACTGGTTTCACATTCACCACCCTGAATTGACTCTCTTCCG 6780

```
6781 GGCGCTATCATGCCATACCGCGAAAGGTTTTGCGCCATTCGATGGTGTCCGGGATCTCGA 6840
6841 CGCTCTCCCTTATGCGACTCCTGCATTAGGAAATTAATACGACTCACTATA 6891
```

Supporting References

1. Young DD, *et al.* (2011) An evolved aminoacyl-tRNA synthetase with atypical polysubstrate specificity. *Biochemistry* **50**(11):1894-1900.
2. Charneau P, *et al.* (1994) HIV-1 reverse transcription. A termination step at the center of the genome. *J Mol Biol* **241**(5):651-662.
3. Hess B, Bekker H, Berendsen HJC, & Fraaije JGEM (1997) LINCS: A linear constraint solver for molecular simulations. *Journal of computational chemistry* **18**(12):1463-1472.
4. Berendsen HJC, Postma JPM, Vangunsteren WF, Dinola A, & Haak JR (1984) Molecular-Dynamics with Coupling to an External Bath. *J Chem Phys* **81**(8):3684-3690.
5. Cingolani G, Petosa C, Weis K, & Müller CW (1999) Structure of importin-beta bound to the IBB domain of importin-alpha. *Nature* **399**(6733):221-229.
6. Lee SJ, *et al.* (2003) The structure of importin-beta bound to SREBP-2: nuclear import of a transcription factor. *Science (New York, NY)* **302**(5650):1571-1575.
7. Lee SJ, Matsuura Y, Liu SM, & Stewart M (2005) Structural basis for nuclear import complex dissociation by RanGTP. *Nature* **435**(7042):693-696.
8. Liu SM & Stewart M (2005) Structural basis for the high-affinity binding of nucleoporin Nup1p to the Saccharomyces cerevisiae importin-beta homologue, Kap95p. *Journal of molecular biology* **349**(3):515-525.
9. Mitrousis G, Olia AS, Walker-Kopp N, & Cingolani G (2008) Molecular basis for the recognition of snurportin 1 by importin beta. *The Journal of biological chemistry* **283**(12):7877-7884.
10. Forwood JK, *et al.* (2010) Quantitative structural analysis of importin-beta flexibility: paradigm for solenoid protein structures. *Structure (London, England : 1993)* **18**(9):1171-1183.
11. Wohlwend D, Strasser A, Dickmanns A, & Ficner R (2007) Structural basis for RanGTP independent entry of spliceosomal U snRNPs into the nucleus. *Journal of molecular biology* **374**(4):1129-1138.